2011/01/17

SARS coronavirus papain-like protease suppressed interferon-α-induced responses through down-regulation of ERK1-mediated signaling pathways

Shih-Wein Li [1,2] Chien-Chen Lai [2,3¶] Jia-Fong Ping[1] Fuu-Jen Tsai[3]

Lei Wan[3] Ying-Ju Lin [3] Szu-Hao Kung [4] Cheng-Wen Lin [1,5,6 *]

[1] Department of Medical Laboratory Science and Biotechnology, China Medical University, Taichung, Taiwan

[2] Institute of Molecular Biology, National Chung Hsing University, Taichung, Taiwan

[3] Department of Medical Genetics and Medical Research, China Medical University Hospital, Taichung, Taiwan

[4] Department of Biotechnology and Laboratory Science in Medicine, National Yang Ming University, Taipei, Taiwan

[5] Clinical Virology Laboratory, Department of Laboratory Medicine, China Medical University Hospital, Taichung, Taiwan

[6] Department of Biotechnology, Asia University, Wufeng**,** Taichung, Taiwan

Running title: SARS CoV PLpro suppressed ERK1/STAT1 signaling

[¶]Co-first author

*Corresponding author: Cheng-Wen Lin, PhD, Professor. Department of Medical Laboratory Science and Biotechnology, China Medical University, No. 91, Hsueh-Shih Road, Taichung 404, Taiwan

Fax: 886-4-22057414

Email: cwlin@mail.cmu.edu.tw

Abstract

SARS coronavirus (SARS-CoV) papain-like protease (PLpro), a deubiquitinating enzyme, reportedly blocks polyI:C-induced activation of IRF3 and NF-κB, reducing interferon (IFN) induction. This study investigated Type I IFN antagonist mechanism of PLpro in human promonocytes. PLpro antagonized IFNα-induced responses such as ISRE- and AP-1-driven promoter activation, PKR, 2'-5'-OAS, IL-6 and IL-8 expression, and STAT1(Tyr701), STAT1(Ser727) and c-Jun phosphorylation. Proteomics approach demonstrated down-regulation of ERK1 and up-regulation of ubiquitin-conjugating enzyme (UBC) E2-25k as inhibitory mechanism of PLpro on IFNα-induced responses. IFNα treatment significantly induced mRNA expression of UBC E2-25k, but not ERK1, causing time-dependent decrease of ERK1, but not ERK2, in PLpro-expressing cells. Poly-ubiquitination of ERK1 showed a relationship between ERK1 and ubiquitin proteasome signaling pathways associated with IFN antagonism by PLpro. Combination treatment of IFNα and proteasome inhibitor MG132 showed a time-dependent restoration of ERK1 protein levels and significant increase of ERK1, STAT1 and c-Jun phosphorylation in PLpro-expressing cells. Importantly, PD098059 (an ERK1/2 inhibitor) treatment significantly reduced IFNα-induced ERK1 and STAT1 phosphorylation, inhibiting IFNα-induced expression of 2'-5'-OAS in vector control cells and PLpro-expressing cells. Overall results proved down-regulation of ERK1 by ubiquitin proteasomes and suppression of interaction between ERK1 and STAT1 as Type I IFN antagonist function of SARS-CoV PLpro.

Keywords: SARS coronavirus, papain-like protease, deubiquitination, interferon-α, ERK1, STAT1

Introduction

Severe acute respiratory syndrome (SARS)-associated coronavirus (SARS-CoV) is a novel pandemic virus causing highly contagious respiratory disease with approximately 10% mortality rate (Hsueh *et al.*, 2004; Lee *et al.*, 2003; Tsang *et al.*, 2003). Pathology entails bronchial epithelial denudation, loss of cilia, multinucleated syncytial cells, squamous metaplasia and transendothelial migration of monocytes/macrophages and neutrophils into lung tissue (Hsueh *et al.*, 2004; Nicholls *et al.*, 2003). Hematological examination reveals lymphopenia, thrombocytopenia and leukopenia (Wang *et al.*, 2004b; Yan *et al.*, 2004) accompanied by rapid elevation in serum of inflammatory cytokines like IFN-gamma, IL-18, TGF-beta, IL-6, IP-10, MCP-1, MIG, and IL-8, which stimulate recruitment of neutrophils, monocytes, and immune responder cells like natural killer (NK), T, and B cells into lungs and other organs (He *et al.*, 2006; Huang *et al.*, 2005; Wong *et al.*, 2004).

SARS-CoV genome is an ~30 kbp positive-stranded RNA with a 5' cap and a 3' poly(A) tract that contains 14 open reading frames (ORFs) (Marra *et al.*, 2003; Rota *et al.*, 2003; Ziebuhr, 2004). The 5' proximal and largest of these ORFs encodes two large overlapping polyproteins replicase 1a and 1ab (~ 450 kDa and ~750 kDa, respectively) processed to produce nonstructural (NS) proteins primarily involved in RNA replication. Two specific embedded proteases, papain-like (PLpro) and 3C-like (3CLpro), mediate processing of 1a and 1ab precursors into 16 NS proteins (termed NS 1 through NS16).

PLpro, located within NS3, cleaves at NS1/2, NS2/3 and NS3/4 boundaries using consensus motif LXGG (Barretto *et al.*, 2005; Lindner *et al.*, 2005; Thiel *et al.*, 2003), along with consensus cleavage sequence of cellular deubiquitinating enzymes. Modeling and crystal structures reveal correlation between SARS-CoV PLpro and the

herpes virus-associated ubiquitin-specific protease (HAUSP), indicating potential deubiquitinating activity (Ratia *et al.*, 2006; Sulea *et al.*, 2005) observed in *in vitro* cleavage assays (Barretto *et al.*, 2005; Lindner *et al.*, 2005). Interestingly, one such *in vitro* deubiquination assay measured the cleavage of ubiquitin-like protein, interferon (IFN)-induced 15-kDa protein (ISG15), from an ISG15-fusion protein, suggesting de-ISGylation by PLpro as a mechanism by which SARS-CoV inactivates IFNα/β-induced innate immune response.

SARS-CoV infection does not induce Type I IFNs in cell culture (Spiegel *et al.*, 2005). Recent reports reveal PLpro inhibiting the phosphorylation of interferon regulatory factor 3 (IRF-3) and Type I IFN synthesis (Devaraj *et al.*, 2007) and antagonizing both IRF-3 and NF-κB signaling pathways (Frieman *et al.*, 2009). Still, mechanisms of Type I IFN antagonism by which SARS-CoV PLpro does this remain unclear. Type I interferons (IFNs, IFNα, IFNβ, and IFNω) mediate a wide range of biological activities: antiviral activity, immune response, differentiation, cell growth, apoptosis (Biron, 2001). IFN-α/β binds to common heterodimeric receptor composed of IFN-α/β Receptor 1 (IFNAR1) and IFN-α/β Receptor 2 (IFNAR2), then activates Janus kinase (JAK) family plus signal transducers and activators of transcription (STATs) family (Tang *et al.*, 2007). Phosphorylation of STAT1 at tyrosine 701 by JAK1 is required for STAT1-STAT2 heterodimer formation and nuclear translocation (Banninger & Reich, 2004). Phosphorylation of STAT1 at serine 727 by ERK1/2 and p38 MAPK facilitates interaction of STAT1 with basal transcription machinery for full expression of antiviral genes like Protein kinase R (PKR), 2’5’-oligoadenylate synthetase (OAS), and IFN-stimulated gene 15 (ISG15) (Deb *et al.*, 2003; Uddin *et al.*, 2002). Currently, IFNα is also a widely used cytokine for treating human solid and haematologic malignancies (Tagliaferri *et al.*, 2005). IFNα-mediated anti-tumor effect

correlates with activation of JAK-STAT signaling pathway, resulting in up-regulation of Fas/FasL and Jnk1/p38 stimulation signaling pathways. Escape mechanisms of IFNα-mediated anti-tumor effect are likewise reported: e.g., EGF-mediated Ras/Raf/ERK1-2–dependent pathway, Akt and NFkB-dependent pathways and STAT3/PI3 K–mediated signaling (Tagliaferri *et al.*, 2005). Some key regulators of signal transduction—e.g., JAK1, STAT1, ERK1—are demonstrably modified by ubiquitin conjugation (Malakhov *et al.*, 2003; Zhimin & Tony, 2009), with over 100 ubiquitin-conjugated proteins encompassing diverse cellular pathways identified in antiviral innate immune responses (Giannakopoulos *et al.*, 2005; Zhao *et al.*, 2005): e.g., NF-κB-inducing kinase (NIK), critical regulator of noncanonical NF-κB pathway, is ubiquitinated and degraded by RING finger E3 ligases (Varfolomeev *et al.*, 2007). With SARS-CoV PLpro as a deubiquitinating enzyme, this points to specifically disrupting signal transduction of innate immune system against SARS-CoV infection.

Investigating possible effect of PLpro on the responses to type I IFNs is vital to understanding SARS pathogenesis. This study first demonstrated stable expression of SARS-CoV PLpro significantly inhibited IFNα-induced responses like ISRE- and AP-1-driven promoter activation, gene expression of PKR, 2'-5'-OAS, IL-6 and IL-8, and phosphorylation of STAT1 and c-Jun. Down-regulation of ERK1 was identified by comparative proteomic analysis of PLpro-expressing vs. control cells with respect to IFNα response, correlating with potential antagonistic mechanism of SARS-CoV PLpro in response to IFNα.

Results

Expression of the SARS-CoV PLpro in human promonocytes

To characterize effect of SARS-CoV PLpro on the intracellular innate

immune response, human promonocyte HL-CZ cells were co-transfected with the plasmid pSARS-CoV PLpro (expressing PLpro with HSV epitope tag) or empty control vector and GFP reporter plasmid followed by two weeks of treatment with G418 to select stably transfected cells**.** Expression of PLpro was detected by immunofluorescent staining (Fig. 1A) and Western blotting (Fig. 1B), with vector-derived HSV-tag found in both empty vector- and pSARS-CoV PLpro-transfected cells and HSV-tag detected only in pSARS-CoV-PLpro-transfected cells. Western blotting of transfected cells' lysates with anti-HSV-tag antibodies revealed a 60-kDa band in pSARS-CoV-PLpro- transfected cells (Fig. 1B), not in empty vector-transfected cells.

To determine if expressed PLpro was active, proteolytic activity in cell lysates was assayed by *in-vitro trans*-cleavage, with HRP containing LXGG motif recognized by PLpro as substrate. Fig. 1C shows significant reduction in HRP enzyme activity in the reaction containing lysates of PLpro-expressing cells, not in reaction with lysates from vector control cells. Lysates of PLpro-expressing cells also exhibited time-dependent *trans*-cleavage activity. SARS-CoV PLpro expressed in human promonocyte cells was thus enzymatically active.

Inhibition of PLpro on IFNα-induced ISRE- and AP-1-mediated activation

To test effect of SARS-CoV PLpro on ISRE-mediated responses to IFNα, activity of ISRE-driven reporter and mRNA expression of ISRE-driven gene PKR in empty vector controls and PLpro-expressing cells were examined by dual luciferase reporter assay system (Fig. 2A) and quantitative real-time RT-PCR (Fig. 2B). Cells were co-transfected with *cis*-reporter plasmid containing firefly luciferase under control of the ISRE and an internal control reporter plasmid that constitutively

expressed renilla luciferase. After treatment with IFNα for 4 h, expression of firefly luciferase was determined and normalized to renilla luciferase expression. Fig. 2A plots vector control and PLpro-expressing cells' dose-dependent transcriptional activity of ISRE promoter by IFNα. ISRE promoter-driven luciferase activity in PLpro-expressing cells was half that in vector control cells. The mRNA expression of specific ISRE-driven gene PKR was analyzed in both types of cells in the absence or presence of IFNα, using quantitative real-time RT-PCR assays (Fig. 2B). Induction of PKR by IFNα was ~7 fold lower in PLpro expressing cells than in control vector cells. Since endogenous PKR promoter contains not only ISRE element but also kinase-conserved sequence (KCS) element for both basal and IFN-inducible PKR promoter activity (Samuel, 2001), the other specific ISRE promoter-driven gene 2'-5'-OAS was further analyzed (Fig. 2C). Induction of 2'-5'-OAS by IFNα was 6-fold lower in PLpro-expressing cells than in vector controls. Results confirmed the antagonism of IFNα–induced ISRE-mediated gene expression by PLpro.

Subsequently, effect of SARS-CoV PLpro on AP-1-mediated responses to IFNα was tested (Fig. 3). Activity of AP-1 enhancer in response to IFNα was next determined by transient transfection with plasmid vector containing luciferase under control of the AP-1 enhancer. Fig. 3A shows luciferase activity significantly induced in a dose-dependent manner in control vector cells by IFNα, but induction using the same level of IFNα totally absent in PLpro-expressing cells. These results indicate SARS-CoV PLpro mediated suppression AP-1-mediated promoter activity in response to IFNα. Upon stimulation with IFNα, a 15-fold increase in IL-6 mRNA was induced in vector control cells; no significant induction occurred in PLpro-expressing cells (Fig. 3B). Since the AP-1 element was also required for the IL-8 expression (Hoffmann *et al.*, 2002), thus IL-8 mRNA levels in response to

IFNα were also measured (Fig. 3C). Levels of IL-8 mRNA were 3.5-fold higher in both unstimulated and stimulated vector controls than in unstimulated and stimulated PLpro-expressing cells (Fig. 3C), suggesting interference by PLpro with basal level IL-8 mRNA transcription. AP-1 promoter activity and driven gene expression indicated SARS-CoV PLpro as significantly inhibiting mRNA expression of AP-1-mediated genes.

Down-regulation of IFNα-induced ERK1-mediated signaling by PLpro

For a global perspective mechanism of Type I IFN antagonism by SARS-CoV PLpro, differential protein expression in vector control and PLpro-expressing cells in the absence or presence of IFNα was analyzed by two-dimensional electrophoresis (2-D) gel and nanoscale capillary liquid chromatography/electrospray ionization Q-TOF MS to identify differentially regulated proteins. In Fig 4A, down-regulated protein extracellular signal-regulated kinase 1 (ERK1) and up-regulated ubiquitin-conjugating enzyme (UBC) E2-25K appeared in 2D gels of IFNα-treated PLpro-expressing cells, and then identified by trypsin digestion and NanoLC Trap Q-TOF MS analysis. ERK1 showed a Mascot score of 109, sequence coverage of 14%, and 2 matched peptides; UBC E2-25K showed a Mascot score of 248, sequence coverage of 59%, and 4 matched peptides. Peptide peaks from Q-TOF MS analysis from two representative spots of ERK1 and UBC E2-25K (Figs. 4B-4C, respectively). ERK1 in particular is reported in several biological pathways (mitogen-activated protein kinase kinase, cytokine-mediated inflammation, IFN signaling pathways) and thus could play an important role in the mechanism of IFNα antagonism by PLpro.

Up-regulation of UBC E2-25K of ubiquitin proteasome pathways by PLpro

Quantitative RT-PCR was employed to determine expression levels of ERK1 and UBC E2-25K in PLpro-expressing and vector control cells in the absence or presence of IFNα (Fig. 5). Amount of ERK1 mRNA showed no difference between vector control and PLpro-expressing cells, whether treated with IFNα or not (Fig. 5A). Relative level of UBC E2-25K mRNA in PLpro-expressing cells was markedly higher than that in vector controls, with or without IFNα treatment (Fig. 5B), proving that SARS-CoV PLpro activates the ubiquitin-proteasome system in human promonocyte cells. To compare ERK1 protein levels in vector control and PLpro-expressing cells in the presence or absence of IFNα, ERK1 and ERK2 were measured by Western blots with anti-p44/p42 (ERK1/2) monoclonal antibody (Fig. 6A). Western blotting showed 42-kDa ERK2 protein levels roughly similar in vector control and PLpro-expressing cells, whereas the protein level of 44-kDa ERK1 in PLpro-expressing cells was near 50% of that in controls (determined by densitometry normalized to β-actin protein control in each sample) (Fig. 6A, Lanes 1-2). IFNα treatment caused time-dependent reduction of ERK1, but not ERK2, in PLpro-expressing cells (Fig. 6A, Lanes 4 and 6). Results confirmed data of 2-D/MALDI TOF MS, which showed definite reduction of ERK1 in PLpro-expressing cells in response to IFNα.

Since PLpro-expressing cells have no difference in mRNA amount, but a significantly reduction of ERK1 protein levels by IFNα, we suggest that up-regulation of UBC E2-25k in PLpro-expressing cells could increase ubiquitination on ERK1, enhancing ERK1 degradation by IFNα treatment. To test the hypothesis, ERK1 immunoprecipition followed by Western blot probed with anti-ubiquitin antibodies was conducted in the absence or presence of IFNα (Fig 6B), revealing that ERK1 conjugated with different sizes of poly-ubiquitin chains: i.e., molecular sizes of 52, 60,

68, 76, and 84 kDa. Higher level of ERK1 ubiquitination was found in PLpro-expressing cells (Fig. 6B, Lane 2) than in vector control cells (Fig. 6B, Lane 1). Moreover, IFNα treatment significantly reduced the level of ERK1 ubiquitination in PLpro-expressing cells (Fig. 6B, Lane 4), not in vector controls (Fig. 6B, Lane 3).

To test correlation between up-regulation of unbiquitin proteasome activity and down-regulation of ERK1 in PLpro-expressing cells, proteasome inhibitor MG-132 was added to analyze changes of ERK1 and ERK2 using Western blot assays with anti-p44/p42 (ERK1/2) monoclonal antibody (Fig. 6C). Treatment with both IFNα and proteasome inhibitor MG-132 caused time-dependent increases of ERK1 and ERK2, in PLpro-expressing cells (Fig 6C, Lanes 2, 4, 6, and 8). The higher expression level of ERK2 than ERK1 was consistently observed in vector control and PLpro-expressing cells in responses to treatment with/without both IFNα and proteasome inhibitor MG-132. The increase of ERK1 level in PLpro-expressing cells correlated with treatment of proteasome inhibitor MG-132, being not compensated by ERK2. After 1 h treatment with both IFNα and MG-132, overall amount of ERK1 in PLpro-expressing cells was equal to that in vector control cells (Fig 6C, Lanes 7 and 8). Results indicate proteasome inhibitor MG-132 blocking escape of IFNα-induced response by ERK1 degradation in PLpro-expressing cells, along with SARS-CoV PLpro enhancing ERK1 degradation by up-regulating ubiquitin proteasome pathways in response to IFNα, being associated with inhibiting IFNα-induced ISRE- and AP-1 promoter activation and IFNα-stimulated gene expression.

Inhibition of ubiquitin proteasome activity restored activation of IFNα-induced ERK-mediating signaling in PLpro-expressing cells

To examine effects of unbiquitin proteasome up-regulation on

ERK1-mediated signaling, proteasome inhibitor MG-132 was added to analyze changes of ERK1-mediated signaling pathway. Phosphorylation of ERK1, STAT1 and c-Jun in PLpro-expressing cells and vector control cells was subsequently analyzed by Western blots with phosphorylation site-specific antibodies (Fig. 7). IFNα treatment caused time-dependent ERK1 phosphorylation in vector controls (Fig. 7A, Lanes 1, 3, 5, and 7), but only a transient period of ERK1 phosphorylation in PLpro-expressing cells (Fig. 7A, Lane 4), probably due to lower ERK1 protein levels via degradation by ubiquitin-proteasome pathway in PLpro-expressing cells following IFNα treatment (Fig. 6). Consistent with this hypothesis, treatment with both IFNα and proteasome inhibitor MG-132 restored IFNα-induced activation of ERK1 in a time-dependent manner in PLpro-expressing cells (Fig. 7B, Lanes 2, 4, 6, and 8). Treatment with IFNα or both IFNα and the proteasome inhibitor MG-132 had no detectable band of phospho-ERK2 in vector control and PLpro-expressing cells. Subsequently, PLpro expression suppressed phosphorylation of STAT1 at Tyr701 and Ser727 sites in resting cells and in response to IFNα treatment (Fig. 7C, Lanes 4, 6, and 8). Treatment with proteasome inhibitor MG-132 also significantly increased phosphorylation of STAT1 at Tyr701 and Ser727 sites in PLpro-expressing cells induced with IFNα (Fig. 7D, Lanes 4, 6, and 8). Moreover, phosphorylation of transcriptional factor c-Jun was assessed to find level of c-Jun phosphorylation similar in both types of cells. Yet IFNα treatment reduced c-Jun phosphorylation, meanwhile treatment with both IFNα and MG-132 also significantly increased c-Jun phosphorylation in PLpro-expressing cells (Figs. 7C and 7D, Lanes 4, 6, and 8). As expected, if PLpro-induced degradation of ERK1 suppresses STAT1 and c-Jun activation, inhibition of ubiquitin proteasome function with MG132 heightened IFNα-induced activation of ERK1-mediated signaling in PLpro-expressing cells.

Correlation of ERK1 phosphorylation with STAT1 signaling pathways

To confirm effect of ERK1 phosphorylation on STAT1 signaling, inhibition of PD098059 (an ERK1/2 inhibitor) on ERK1 and STAT1 phosphorylation was analyzed by Western blotting (Fig. 8). PD098059 treatment had inhibitory effects on IFNα-induced ERK1 phosphorylation in vector control cells and PLpro-expressing cells (Fig. 8A, Lanes 5-7; Fig. 8B, Lanes 5-7). Importantly, PD098059 treatment also manifests inhibitory effects on STAT1 phosphorylation at Ser727, but not Tyr701 in vector control cells and PLpro-expressing cells in response to IFNα treatment (Fig. 8A, Lanes 5-7; Fig. 8B, Lanes 5-7). In addition, effects of PD098059 treatment on IFNα-induced ISRE promoter-driven gene expression were further investigated using real time RT-PCR (Supplemental Fig. 1). PD098059 treatment starkly reduced IFNα-induced expression of 2'-5'-OAS in vector control and PLpro-expressing cells (Supplemental Fig. 1). Results confirmed a link between ERK1 activation and STAT1 signaling as the antagonism of IFNα–induced ISRE-mediated gene expression by PLpro.

Discussion

SARS-CoV does not induce type I IFN in cell culture, which may be crucial to pathogenesis of this virus. This study focused on one SARS-CoV protein, PLpro protease, earlier reported to have antagonistic activity in innate immune responses including synthesis of IFNs and cytokines (Devaraj *et al.*, 2007; Frieman *et al.*, 2009). We first demonstrated stable SARS-CoV PLpro expression in human promonocyte cells as well as inhibition of IFNα-induced ISRE- and AP-1-driven promoter activity and reduction of IFN-stimulated gene expression (Figs. 2-3). Results concurred with

previous findings: SARS-CoV PLpro protein inhibited activity of IFNβ, ISRE and NF-κB promoters induced by polyI:C (Devaraj *et al.*, 2007; Frieman *et al.*, 2009). The antagonistic mechanism of SARS-CoV PLpro on these activities is controversial (Devaraj *et al.*, 2007; Frieman *et al.*, 2009). Devaraj and colleagues demonstrated PLpro interacting with IRF-3, blocking phosphorylation and nuclear translocation of IRF-3 and disrupting activation of Type I IFN responses (Devaraj *et al.*, 2007). Frieman and colleagues found PLpro not directly binding with IRF-3 or inhibiting *in vitro* phosphorylation of IRF-3 (Frieman *et al.*, 2009).

This study used proteomic approach to detect changes in protein expression in PLpro-expressing cells in the presence or absence of IFNα (Fig. 4). PLpro expression in human promonocyte cells stimulated mRNA expression of UBC E2-25K (Fig. 5B), which could support increase of protein level of UBC E2-25K in 2-D gels (Fig. 4). PLpro expression caused 50% decrease of ERK1, but not ERK2, in PLpro-expressing cells compared to vector controls (Fig 6A), being associated with ubiquitin-dependent proteosomal degradation of ERK1, as confirmed by poly-ubiquitination of ERK1 and treatment with proteosome inhibitor MG132 (Figs. 6B-6C). IFNα treatment enhanced time-dependent manner of ERK1 down-regulation, but proteosome inhibitor MG132 time-dependently restored IFNα-enhanced degradation of ERK1 in PLpro-expressing cells, but not vector controls (Figs. 6A and 6C). With ERK1/2 signaling regulated by ubiquitin-proteasome system via degradation of ERK1/2 and the upstream MEKK1 by ubiquitination (Laine & Ronai, 2005; Lu *et al.*, 2002), those reports led us to identify ERK1 ubiquitination level in vector control and PLpro-expressing cells with or without IFNα treatment (Fig. 6B). Interestingly, PLpro expression significantly increased ERK1 ubiquitination with poly-ubiquitin chains compared to vector control cells (Fig. 6B, Lanes 1-2), while

IFNα treatment decreased ubiquitinated levels and protein amounts of ERK1 in PLpro-expressing cells, not in vector control cells (Fig. 6B, Lanes 3-4). Treatment with proteasome inhibitor MG132 restored protein amounts of ERK1 (Fig. 6C) and IFNα-induced activation of ERK1-mdiated signaling in PLpro-expressing cells (Fig 8), in concordance with prior studies: i.e., ERK1/2 signaling regulated by ubiquitin-proteasome system via degradation of ERK1/2 and upstream MEKK1 by ubiquitination (Laine & Ronai, 2005; Lu *et al.*, 2002). Proteomic analysis identified down-regulation of ERK1 that was ubiquitinated and degraded by up-regulation of ubiquitin proteasome pathways in PLpro-expressing cells, being responsible for the mechanism of IFNα antagonism by SARS-CoV PLpro.

The treatment with proteasome inhibitor MG132 reversed this inhibition of IFNα-induced ERK1-mediated signaling by PLpro (Fig. 7), indicating a significant correlation between ERK1 and STAT1 in PLpro-expressing cells in response to IFNα. Results concurred with prior studies, with phosphorylation at Serine 727 of STAT1 by active ERK1 involved in IFNα/β-induced response (Wang *et al.*, 2004a) and IFNγ inflammatory response (Lombardi *et al.*, 2008; Matsumoto *et al.*, 2005). In addition, down-regulation of ERK1 in PLpro-expression cells correlated with suppression of AP-1-driven luciferase activity, IL-6 and IL-8 mRNA expression and c-Jun phosphorylation in responses to IFNβ (Figs. 3 and 7). Importantly, we confirmed the correlation of ERK1 and STAT1 signaling pathways by treatment of PD098059 (an ERK1/2 inhibitor) (Fig. 8). PD098059 treatment inhibited IFNα-induced ERK1 and STAT1 phosphorylation in vector control and PLpro-expressing cells, as well as IFNα-induced expression of 2'-5'-OAS in vector control and PLpro-expressing cells (Supplemental Fig. 1). In addition, the other ERK1/2 inhibitor U0126 was used to test the correlation between ERK1/2 and STAT1. ERK1/2 inhibitor U0126

significantly inhibited IFN-alpha-induced phosphorylation of STAT1 at Ser727 in vector control cells and PLpro-expressing cells (Supplemental Fig. 2). ERK1/2-mediated signaling proves elemental in EGF-induced survival response to antagonize IFNα-induced apoptosis of cancer cells (Caraglia *et al.*, 2003). Down-regulation of ERK1-mediated signaling by PLpro might thus be considered in escape mechanism of SARS-CoV against Type I IFNs. Activation of ERK1-mediated signaling may improve innate immune response against SARS-CoV, being alternative targets for development of SARS therapy.

We also demonstrated reduction of ERK1 protein level in human promonocyte cells 24 hours post infection with human coronavirus NL63 (HCoV-NL63) and reversion of ERK1 protein level in HCoV-NL63-infected cells after a 24-hour incubation of IFNα and proteasome inhibitor MG132 (Supplemental Fig. 3). In addition, the reduction of IFNα-induced phosphorylation of both ERK1 and STAT1 at Ser727 was confirmed in human lung adenocarcinoma epithelial A549 cells expressing SARS-CoV PLpro compared to vector control (Supplemental Fig. 4). Surprisingly, ERK2 that had the consistently higher expression level than ERK1 in vector control and PLpro-expressing cells showed fewer amounts of protein level and IFNα-induced phosphorylation in PLpro-expressing cells than vector control cells (Figs. 6A, 7A, and 8, Supplemental Fig. 4). The treatment with proteasome inhibitor MG132 reversed the amounts of ERK2 protein and the inhibition of IFNα-induced ERK2 phosphorylation in PLpro-expressing cells (Figs. 6C and 7B). Besides ERK1, ERK2 might be involved in Type I IFN antagonism by SARS-CoV PLpro. ERK1 and ERK2 have approximately 85% of amino acid identity co-expressed in virtually all tissues but with remarkably variable relative abundance, ERK2 as the predominant isoform in brain and hematopoietic cells (Milella *et al.*, 2003; Pages & Pouyssegur,

2004). Recent evidence suggests possible quantitative difference in ERK1 and ERK2 dynamics that could have a significant role in their regulation. Ectopic expression of ERK1, albeit not ERK2, attenuates Ras-dependent tumor formation in nude mice (Vantaggiato *et al.*, 2006). The properties of their cytoplasmic-nuclear trafficking showed ERK1 shuttles between nucleus and cytoplasm at a much slower rate than ERK2, correlating with reduced capability of ERK1 to carry proliferative signals to the nucleus (Marchi *et al.*, 2008). Constitutive activation of ERK2, but not ERK1, is critical for the acquired resistance to Imatinib Mesylate in chronic myelogenous leukemia management (Aceves-Luquero *et al.*, 2009). In addition to cancers, Ebola virus envelope glycoprotein reduced phosphorylation and kinase activity of ERK2, but not ERK1, correlating with induction of cell death (Zampieri *et al.*, 2007). Vaccinia virus M2L protein blocks ERK2 phosphorylation, inhibiting virus-induced NF-κB activation (Gedey *et al.*, 2006). Type I IFN antagonism of SARS-CoV PLpro via ERK1 down-regulation might thus be a unique mechanism useful in developing therapeutic agents against SARS-CoV infection.

In conclusion, stable SARS-CoV PLpro expression significantly suppressed IFNα-induced responses. Up-regulation of ubiquitin-proteasome pathway by SARS-CoV PLpro correlated with increase of ERK1 ubiquitination. IFNα treatment elicited ERK1 degradation, then down-regulated ERK1-mediated signaling in PLpro-expressing cells, resulting in negative regulation of STAT1 and AP-1 signaling pathways. Importantly, inhibition of ubiquitin proteasome function with MG132 restored IFNα-induced phosphorylation of ERK1, STAT1, and c-Jun, all suppressed by SARS-CoV PLpro. PD098059 treatment confirmed linkage between ERK1 activation and STAT1 signaling pathways as Type I IFN antagonism by PLpro. Moreover, the study may provide novel insight into the molecular mechanism of IFN

antagonism by SARS CoV PLpro.

Materials and methods

Cell culture and transfection

The SARS-CoV PLpro gene, located between nucleotides 4507-5840 of the SARS-CoV TW1 strain genome (GenBank Accession No. AY291451), was amplified by RT-PCR from genome RNA template, using primers 5'-CTCCGAAT TCAACTCTCTAAATGAGCCGCTTGTC-3' and 5'-GAGGCTCGAGATCCTCTGG GTCTTCAGGAGCGAGTTCTGGCTGTACGACACAGGCTTGATGGTTGTAGT G-3'. Forward primer contained *Eco*RI restriction site; reverse primer included an *Xho*I restriction site and HSV epitope tag. Amplified RT-PCR product was cloned into pcDNA3.1/His C vector (Invitrogen), resulting construct named pSARS-CoV PLpro. The pSARS-CoV PLpro (4.5 μg) plus indicator vector pEGFP-N1 (0.5 μg) (Clontech) or pcDNA3.1 empty vector plus pEGFP-N1 were transfected into HL-CZ cells (human promonocyte cell line) with GenePorter reagent. As per manufacturer's direction (Gene Therapy Systems, San Diego, CA), transfected cells were incubated for 5 hours with a mixture of plasmid DNA and GenePorter reagent, then maintained in RPMI 1640 medium containing 20% bovine serum (FBS). For the selection of the stably transfected cell line, cells were incubated with RPMI 1640 medium containing 10 % FBS and 800 μg/ml of G418. PLpro expression was detected by Western blotting of transfected cell lysates, using anti-HSV Tag mAb (Novagen) as a probe.

In vitro trans-cleavage activity of SARS-CoV PLpro

The protease activity in SARS-CoV PLpro-transfected cells was determined by spectrophotometrically following digestion of substrate horseradish peroxidase (HRP)

containing the LXGG motif (Sigma). 150 µl of transfected cell lysates were added to 150 µl of substrate reagent containing 0.01 µg/ml HRP in 50 mM Tris-HCl. After 1-, 2-, 3-, and 4-h incubation at 37℃, reaction mixtures were added to a 96-well plate and non-digested HRP activity measured by adding chromogen solution containing 2,2'-azino-di-3- ethylbenzthiazoline-6-sulfonate (ABTS) and hydrogen peroxide. Relative *trans*-cleavage activity was calculated as $1 - (A405_{PLpro})/(A405_{no\ PLpro})$.

Transient transfections of *cis*-reporter plasmids for signaling pathway assays

Plasmid pISRE-Luc *cis*-reporter was purchased from Stratagene. SARS-CoV PLpro-expressing and empty vector control cells were transfected with *cis*-reporter plasmid indicated, plus internal control reporter pRluc-C1 (BioSignal Packard) using GenePorter reagent. After 4 h incubation with or without IFNα2 (Hoffmann-La Roche), activity of experimental firefly luciferase and control renilla luciferase was gauged by dual Luciferase Reporter Assay System (Promega) and TROPIX TR-717 Luminometer (Applied Biosystems) described by Lin *et al.* (Lin *et al.*, 2008).

2-DE and protein spot analysis

For two-dimensional gel electrophoresis, empty vector control cells and PLpro-expressing cells incubated for 3 days in the presence or absence of 3000 U/ml IFNα were harvested, washed twice with ice-cold phosphate-buffered saline, and then extracted with lysis buffer containing 8 M urea, 4% CHAPS, 2% pH 3-10 non-linear (NL) IPG buffer (GE Healthcare), plus Complete, Mini, EDTA-free protease inhibitor mixture (Roche). After 3 h incubation at 4℃, cell lysates were centrifuged for 15 min

at 16000 g. Protein concentration of resulting supernatants was gauged with Bio-Rad Protein Assay (Bio-Rad, Hercules, CA, USA), 100 μg of protein sample diluted with 350 μl of rehydration buffer (8 M urea, 2% CHAPS, 0.5% IPG buffer pH 3-10 NL, 18 mM dithiothreilol, 0.002% bromophenol blue), then applied to nonlinear Immobiline DryStrips (17 cm, pH 3-10; GE Healthcare). First-dimensional isoelectric focus and second-dimensional electrophoresis were detailed in Lai *et al.* (2007), as was in-gel digestion to recover peptides from gel spots for nanoelectrospray mass spectrometry.

Nanoelectrospray mass spectrometry, data interpretation and database search

Proteins in spots of interest were identified using an Ultimate capillary LC system (LC Packings, Amsterdam, The Netherlands) coupled to a QSTARXL quadrupole-time of flight (Q-TOF) mass spectrometer (Applied Biosystem/MDS Sciex, Foster City, CA, USA). The nanoelectrospray mass spectrometry and database search were described previously (Lai *et al.*, 2007). Protein function and subcellular location were annotated by Swiss-Prot (http://us.expasy.org/sprot/) and proteins categorized according to their biological process and pathway, using the PANTHER Classification system (http://www.pantherdb.org) described in prior studies (Lai *et al.*, 2007; Varfolomeev *et al.*, 2007; Wang *et al.*, 2004a; Wang *et al.*, 2004b).

Western blotting and immunoprecipitation assays

To determine protein expression, lysates of PLpro-expressing cells and empty vector control cells incubated for 1 day in the presence or absence of 3000 U/ml IFNα were mixed 1:1 with 2X SDS-PAGE sample buffer without 2-mercaptoethanol and boiled for 10 min. Proteins in the lysates were resolved by SDS-PAGE and transferred to nitrocellulose. Resulting blots were blocked with

5% skim milk, then reacted with appropriately diluted antibodies, including rabbit anti-STAT 1 (Cell Signaling), rabbit anti-phospho STAT 1 (Ser 727) (Abcam), rabbit anti-phospho STAT 1 (Tyr 701) (Abcam), anti-ERK1/2 mAb (Cell Signaling), anti-phospho-ERK1/2 mAb (Cell Signaling), rabbit anti-c-Jun (Abcam), rabbit anti-phospho c-Jun (Abacm), and anti-ubiquitin mAb (Zymed). Immune complexes were detected with horseradish peroxidase-conjugated goat anti-mouse or anti-rabbit IgG antibodies, followed by enhanced chemiluminescence detection (Amersham Pharmacia Biotech). To detect ubiquitination of ERK1, cell lysates were harvested and incubated with anti-ERK1 antibody for 4 h at 4℃, followed by addition of protein A-Sepharose beads and additional 2 h of incubation. After collection by centrifugation, pellets were washed four times with NET buffer (150 mM NaCl, 0.1 mM EDTA, 30 mM Tris-HCl, pH 7.4); immunoprecipitated proteins were dissolved in 2X SDS-PAGE sample buffer without 2-mercaptoethanol and boiled for 10 min. Proteins were resolved by SDS-PAGE and transferred to nitrocellulose. Resulting blots were blocked with 5% skim milk and then probed with rabbit anti-ERK1 (Zymed) and anti-ubiquitin mAb (Zymed) followed by enhanced chemiluminescence detection.

Quantification of IFNβ mRNA using real time RT-PCR

Total RNA was isolated from PLpro-expressing cells and empty vector control cells incubated for 4 hrs in the presence or absence of 3000 U/ml IFNα, using PureLink Micro-to-Midi Total RNA Purification System Kit (Invitrogen). cDNA was synthesized from 1000 ng of total RNA, using oligonucleotide dT primer and SuperScript III reverse transcriptase kit (Invitrogen). To gauge expression in response

to IFNα, a two-step RT-PCR using SYBR Green I was used. Oligonucleotide primer pairs were (1) forward primer 5'-CAACCAGCGGTTGACTTTTT-3' and reverse primer 5'-ATCCAGGAAGGCAAACTGAA-3' for human PKR, (2) forward primer 5'-GATGTGCTGCCTGCCTTT-3' and reverse primer 5'- TTGGGGGTTAGGTTT ATAGCTG-3' for human 2'-5'-OAS, (3) forward primer 5'-GATGGATGCTTCCAAT CTGGAT-3' and reverse primer 5'- AGTTCTCCATAGAGAACAACATA-3' for human IL-6, (4) forward primer 5'- CGA TGTCAGTGCATAAAGACA -3' and reverse primer 5'- TGAATTCTCAGCCCT CTTCAAAAA-3' for human IL-8, (5) forward primer 5'-CTTCCCTGGCAAGCACTACC-3' and reverse primer 5'-GTTTCGGGCTTCATGTTGA-3' for human ERK1, and (6) forward primer 5'-GCAATGACTCTCCGCACGG-3' and reverse primer 5'-TCTGTTGCAGTCTCT ACATCCC-3' for human UBC E2-25K. In addition, glyceraldehyde-3-phosphate dehydrogenase (GAPDH) mRNA, a housekeeping gene, was measured using 5'-AGCCACATCGCTCAGACAC-3' and 5'-GCCCCA ATACGACCAAATCC-3' as forward and reverse primers. Real-time PCR reaction mixture contained 2.5 μl of cDNA (reverse transcription mixture), 200 nM of each primer in SYBR Green I master mix (LightCycler TaqMAn Master, Roche Diagnostics). PCR was performed with amplification protocol consisting of 1 cycle at 50℃ for 2 min, 1 cycle at 95℃for 10 min, 45 cycles at 95℃ for 15 sec, and 60℃ for 1 min. Amplification and detection of specific products were conducted in ABI PRISM 7700 sequence detection system (PE Applied Biosystems). Relative changes in mRNA level of indicated genes were normalized relative to GAPDH mRNA.

Statistical analysis

Student's t-test or Chi-square test analyzed all data. Statistical significance between vector-control cells and PLpro-expressing cells was noted at $p < 0.05$.

Acknowledgment

We would like to thank the National Science Council (Taiwan) and China Medical University for financial support (NSC96-2320-B-039-008-MY3 and CMU98-CT-22, CMU98-D-S-05, CMU98-P-03).

References

Aceves-Luquero, C. I., Agarwal, A., Callejas-Valera, J. L., Arias-Gonzalez, L., Esparis-Ogando, A., del Peso Ovalle, L., Bellon-Echeverria, I., de la Cruz-Morcillo, M. A., Galan Moya, E. M., Moreno Gimeno, I., Gomez, J. C., Deininger, M. W., Pandiella, A. & Sanchez Prieto, R. (2009). ERK2, but not ERK1, mediates acquired and "de novo" resistance to imatinib mesylate: implication for CML therapy. *PLoS One* **4**, e6124.

Banninger, G. & Reich, N. C. (2004). STAT2 nuclear trafficking. *J Biol Chem* **279**, 39199-39206.

Barretto, N., Jukneliene, D., Ratia, K., Chen, Z., Mesecar, A. D. & Baker, S. C. (2005). The papain-like protease of severe acute respiratory syndrome coronavirus has deubiquitinating activity. *J Virol* **79**, 15189-15198.

Biron, C. A. (2001). Interferons alpha and beta as immune regulators--a new look. *Immunity* **14**, 661-664.

Caraglia, M., Tagliaferri, P., Marra, M., Giuberti, G., Budillon, A., Gennaro, E. D., Pepe, S., Vitale, G., Improta, S., Tassone, P., Venuta, S., Bianco, A. R. & Abbruzzese, A. (2003). EGF activates an inducible survival response via the RAS-> Erk-1/2 pathway to counteract interferon-alpha-mediated apoptosis in epidermoid cancer cells. *Cell Death Differ* **10**, 218-229.

Deb, D. K., Sassano, A., Lekmine, F., Majchrzak, B., Verma, A., Kambhampati, S., Uddin, S., Rahman, A., Fish, E. N. & Platanias, L. C. (2003). Activation of protein kinase C delta by IFN-gamma. *J Immunol* **171**, 267-273.

Devaraj, S. G., Wang, N., Chen, Z., Tseng, M., Barretto, N., Lin, R., Peters, C. J., Tseng, C. T., Baker, S. C. & Li, K. (2007). Regulation of IRF-3-dependent innate immunity by the papain-like protease domain of the severe acute respiratory syndrome coronavirus. *J Biol Chem* **282**, 32208-32221.

Frieman, M., Ratia, K., Johnston, R. E., Mesecar, A. D. & Baric, R. S. (2009). Severe acute respiratory syndrome coronavirus papain-like protease ubiquitin-like domain and catalytic domain regulate antagonism of IRF3 and NF-kappaB signaling. *J Virol* **83**, 6689-6705.

Gedey, R., Jin, X. L., Hinthong, O. & Shisler, J. L. (2006). Poxviral regulation of the host NF-kappaB response: the vaccinia virus M2L protein inhibits induction of NF-kappaB activation via an ERK2 pathway in virus-infected

human embryonic kidney cells. *J Virol* **80**, 8676-8685.

Giannakopoulos, N. V., Luo, J. K., Papov, V., Zou, W., Lenschow, D. J., Jacobs, B. S., Borden, E. C., Li, J., Virgin, H. W. & Zhang, D. E. (2005). Proteomic identification of proteins conjugated to ISG15 in mouse and human cells. *Biochem Biophys Res Commun* **336**, 496-506.

He, L., Ding, Y., Zhang, Q., Che, X., He, Y., Shen, H., Wang, H., Li, Z., Zhao, L., Geng, J., Deng, Y., Yang, L., Li, J., Cai, J., Qiu, L., Wen, K., Xu, X. & Jiang, S. (2006). Expression of elevated levels of pro-inflammatory cytokines in SARS-CoV-infected ACE2+ cells in SARS patients: relation to the acute lung injury and pathogenesis of SARS. *J Pathol* **210**, 288-297.

Hoffmann, E., Dittrich-Breiholz, O., Holtmann, H. & Kracht, M. (2002). Multiple control of interleukin-8 gene expression. *J Leukoc Biol* **72**, 847-855.

Hsueh, P. R., Chen, P. J., Hsiao, C. H., Yeh, S. H., Cheng, W. C., Wang, J. L., Chiang, B. L., Chang, S. C., Chang, F. Y., Wong, W. W., Kao, C. L. & Yang, P. C. (2004). Patient data, early SARS epidemic, Taiwan. *Emerg Infect Dis* **10**, 489-493.

Huang, K. J., Su, I. J., Theron, M., Wu, Y. C., Lai, S. K., Liu, C. C. & Lei, H. Y. (2005). An interferon-gamma-related cytokine storm in SARS patients. *J Med Virol* **75**, 185-194.

Lai, C. C., Jou, M. J., Huang, S. Y., Li, S. W., Wan, L., Tsai, F. J. & Lin, C. W. (2007). Proteomic analysis of up-regulated proteins in human promonocyte cells expressing severe acute respiratory syndrome coronavirus 3C-like protease. *Proteomics* **7**, 1446-1460.

Laine, A. & Ronai, Z. (2005). Ubiquitin chains in the ladder of MAPK signaling. *Sci STKE* **2005**, re5.

Lee, N., Hui, D., Wu, A., Chan, P., Cameron, P., Joynt, G. M., Ahuja, A., Yung, M. Y., Leung, C. B., To, K. F., Lui, S. F., Szeto, C. C., Chung, S. & Sung, J. J. (2003). A major outbreak of severe acute respiratory syndrome in Hong Kong. *N Engl J Med* **348**, 1986-1994.

Lin, C. W., Wu, C. F., Hsiao, N. W., Chang, C. Y., Li, S. W., Wan, L., Lin, Y. J. & Lin, W. Y. (2008). Aloe-emodin is an interferon-inducing agent with antiviral activity against Japanese encephalitis virus and enterovirus 71. *Int J Antimicrob Agents* **32**, 355-359.

Lindner, H. A., Fotouhi-Ardakani, N., Lytvyn, V., Lachance, P., Sulea, T. & Menard, R. (2005). The papain-like protease from the severe acute respiratory syndrome coronavirus is a deubiquitinating enzyme. *J Virol* **79**, 15199-15208.

Lombardi, A., Cantini, G., Piscitelli, E., Gelmini, S., Francalanci, M., Mello, T., Ceni, E., Varano, G., Forti, G., Rotondi, M., Galli, A., Serio, M. & Luconi, M. (2008). A new mechanism involving ERK contributes to rosiglitazone inhibition of tumor necrosis factor-alpha and interferon-gamma inflammatory effects in human endothelial cells. *Arterioscler Thromb Vasc Biol* **28**, 718-724.

Lu, Z., Xu, S., Joazeiro, C., Cobb, M. H. & Hunter, T. (2002). The PHD domain of MEKK1 acts as an E3 ubiquitin ligase and mediates ubiquitination and degradation of ERK1/2. *Mol Cell* **9**, 945-956.

Malakhov, M. P., Kim, K. I., Malakhova, O. A., Jacobs, B. S., Borden, E. C. & Zhang, D. E. (2003). High-throughput immunoblotting. Ubiquitiin-like protein ISG15 modifies key regulators of signal transduction. *J Biol Chem* **278**, 16608-16613.

Marchi, M., D'Antoni, A., Formentini, I., Parra, R., Brambilla, R., Ratto, G. M. & Costa, M. (2008). The N-terminal domain of ERK1 accounts for the

functional differences with ERK2. *PLoS One* **3**, e3873.

Marra, M. A., Jones, S. J., Astell, C. R., Holt, R. A., Brooks-Wilson, A., Butterfield, Y. S., Khattra, J., Asano, J. K., Barber, S. A., Chan, S. Y., Cloutier, A., Coughlin, S. M., Freeman, D., Girn, N., Griffith, O. L., Leach, S. R., Mayo, M., McDonald, H., Montgomery, S. B., Pandoh, P. K., Petrescu, A. S., Robertson, A. G., Schein, J. E., Siddiqui, A., Smailus, D. E., Stott, J. M., Yang, G. S., Plummer, F., Andonov, A., Artsob, H., Bastien, N., Bernard, K., Booth, T. F., Bowness, D., Czub, M., Drebot, M., Fernando, L., Flick, R., Garbutt, M., Gray, M., Grolla, A., Jones, S., Feldmann, H., Meyers, A., Kabani, A., Li, Y., Normand, S., Stroher, U., Tipples, G. A., Tyler, S., Vogrig, R., Ward, D., Watson, B., Brunham, R. C., Krajden, M., Petric, M., Skowronski, D. M., Upton, C. & Roper, R. L. (2003). The Genome sequence of the SARS-associated coronavirus. *Science* **300**, 1399-1404.

Matsumoto, S., Hara, T., Hori, T., Mitsuyama, K., Nagaoka, M., Tomiyasu, N., Suzuki, A. & Sata, M. (2005). Probiotic Lactobacillus-induced improvement in murine chronic inflammatory bowel disease is associated with the down-regulation of pro-inflammatory cytokines in lamina propria mononuclear cells. *Clin Exp Immunol* **140**, 417-426.

Milella, M., Kornblau, S. M. & Andreeff, M. (2003). The mitogen-activated protein kinase signaling module as a therapeutic target in hematologic malignancies. *Rev Clin Exp Hematol* **7**, 160-190.

Nicholls, J. M., Poon, L. L., Lee, K. C., Ng, W. F., Lai, S. T., Leung, C. Y., Chu, C. M., Hui, P. K., Mak, K. L., Lim, W., Yan, K. W., Chan, K. H., Tsang, N. C., Guan, Y., Yuen, K. Y. & Peiris, J. S. (2003). Lung pathology of fatal severe acute respiratory syndrome. *Lancet* **361**, 1773-1778.

Pages, G. & Pouyssegur, J. (2004). Study of MAPK signaling using knockout mice. *Methods Mol Biol* **250**, 155-166.

Ratia, K., Saikatendu, K. S., Santarsiero, B. D., Barretto, N., Baker, S. C., Stevens, R. C. & Mesecar, A. D. (2006). Severe acute respiratory syndrome coronavirus papain-like protease: structure of a viral deubiquitinating enzyme. *Proc Natl Acad Sci U S A* **103**, 5717-5722.

Rota, P. A., Oberste, M. S., Monroe, S. S., Nix, W. A., Campagnoli, R., Icenogle, J. P., Penaranda, S., Bankamp, B., Maher, K., Chen, M. H., Tong, S., Tamin, A., Lowe, L., Frace, M., DeRisi, J. L., Chen, Q., Wang, D., Erdman, D. D., Peret, T. C., Burns, C., Ksiazek, T. G., Rollin, P. E., Sanchez, A., Liffick, S., Holloway, B., Limor, J., McCaustland, K., Olsen-Rasmussen, M., Fouchier, R., Gunther, S., Osterhaus, A. D., Drosten, C., Pallansch, M. A., Anderson, L. J. & Bellini, W. J. (2003). Characterization of a novel coronavirus associated with severe acute respiratory syndrome. *Science* **300**, 1394-1399.

Samuel, C. E. (2001). Antiviral actions of interferons. *Clin Microbiol Rev* **14**, 778-809, table of contents.

Spiegel, M., Pichlmair, A., Martinez-Sobrido, L., Cros, J., Garcia-Sastre, A., Haller, O. & Weber, F. (2005). Inhibition of Beta interferon induction by severe acute respiratory syndrome coronavirus suggests a two-step model for activation of interferon regulatory factor 3. *J Virol* **79**, 2079-2086.

Sulea, T., Lindner, H. A., Purisima, E. O. & Menard, R. (2005). Deubiquitination, a new function of the severe acute respiratory syndrome coronavirus papain-like protease? *J Virol* **79**, 4550-4551.

Tagliaferri, P., Caraglia, M., Budillon, A., Marra, M., Vitale, G., Viscomi, C.,

Masciari, S., Tassone, P., Abbruzzese, A. & Venuta, S. (2005). New pharmacokinetic and pharmacodynamic tools for interferon-alpha (IFN-alpha) treatment of human cancer. *Cancer Immunol Immunother* **54**, 1-10.

Tang, X., Gao, J. S., Guan, Y. J., McLane, K. E., Yuan, Z. L., Ramratnam, B. & Chin, Y. E. (2007). Acetylation-dependent signal transduction for type I interferon receptor. *Cell* **131**, 93-105.

Thiel, V., Ivanov, K. A., Putics, A., Hertzig, T., Schelle, B., Bayer, S., Weissbrich, B., Snijder, E. J., Rabenau, H., Doerr, H. W., Gorbalenya, A. E. & Ziebuhr, J. (2003). Mechanisms and enzymes involved in SARS coronavirus genome expression. *J Gen Virol* **84**, 2305-2315.

Tsang, K. W., Ho, P. L., Ooi, G. C., Yee, W. K., Wang, T., Chan-Yeung, M., Lam, W. K., Seto, W. H., Yam, L. Y., Cheung, T. M., Wong, P. C., Lam, B., Ip, M. S., Chan, J., Yuen, K. Y. & Lai, K. N. (2003). A cluster of cases of severe acute respiratory syndrome in Hong Kong. *N Engl J Med* **348**, 1977-1985.

Uddin, S., Sassano, A., Deb, D. K., Verma, A., Majchrzak, B., Rahman, A., Malik, A. B., Fish, E. N. & Platanias, L. C. (2002). Protein kinase C-delta (PKC-delta) is activated by type I interferons and mediates phosphorylation of Stat1 on serine 727. *J Biol Chem* **277**, 14408-14416.

Vantaggiato, C., Formentini, I., Bondanza, A., Bonini, C., Naldini, L. & Brambilla, R. (2006). ERK1 and ERK2 mitogen-activated protein kinases affect Ras-dependent cell signaling differentially. *J Biol* **5**, 14.

Varfolomeev, E., Blankenship, J. W., Wayson, S. M., Fedorova, A. V., Kayagaki, N., Garg, P., Zobel, K., Dynek, J. N., Elliott, L. O., Wallweber, H. J., Flygare, J. A., Fairbrother, W. J., Deshayes, K., Dixit, V. M. & Vucic, D. (2007). IAP antagonists induce autoubiquitination of c-IAPs, NF-kappaB activation, and TNFalpha-dependent apoptosis. *Cell* **131**, 669-681.

Wang, J. Y., Lee, C. H., Cheng, S. L., Chang, H. T., Hsu, Y. L., Wang, H. C. & Chu, S. H. (2004a). Comparison of the clinical manifestations of severe acute respiratory syndrome and Mycoplasma pneumoniae pneumonia. *J Formos Med Assoc* **103**, 894-899.

Wang, W. K., Chen, S. Y., Liu, I. J., Kao, C. L., Chen, H. L., Chiang, B. L., Wang, J. T., Sheng, W. H., Hsueh, P. R., Yang, C. F., Yang, P. C. & Chang, S. C. (2004b). Temporal relationship of viral load, ribavirin, interleukin (IL)-6, IL-8, and clinical progression in patients with severe acute respiratory syndrome. *Clin Infect Dis* **39**, 1071-1075.

Wong, C. K., Lam, C. W., Wu, A. K., Ip, W. K., Lee, N. L., Chan, I. H., Lit, L. C., Hui, D. S., Chan, M. H., Chung, S. S. & Sung, J. J. (2004). Plasma inflammatory cytokines and chemokines in severe acute respiratory syndrome. *Clin Exp Immunol* **136**, 95-103.

Yan, H., Xiao, G., Zhang, J., Hu, Y., Yuan, F., Cole, D. K., Zheng, C. & Gao, G. F. (2004). SARS coronavirus induces apoptosis in Vero E6 cells. *J Med Virol* **73**, 323-331.

Zampieri, C. A., Fortin, J. F., Nolan, G. P. & Nabel, G. J. (2007). The ERK mitogen-activated protein kinase pathway contributes to Ebola virus glycoprotein-induced cytotoxicity. *J Virol* **81**, 1230-1240.

Zhao, C., Denison, C., Huibregtse, J. M., Gygi, S. & Krug, R. M. (2005). Human ISG15 conjugation targets both IFN-induced and constitutively expressed proteins functioning in diverse cellular pathways. *Proc Natl Acad Sci U S A* **102**, 10200-10205.

Zhimin, L. & Tony, H. (2009). Degradation of activated protein kinases by

ubiquitination. *Annu Rev Biochem* **78**, 435-475.
Ziebuhr, J. (2004). Molecular biology of severe acute respiratory syndrome coronavirus. *Curr Opin Microbiol* **7**, 412-419.

Figure captions

Fig. 1. Expression of SARS-CoV PLpro in human promonocyte HL-CZ cells. Cells transfected with pcDNA3.1 (control vector) plus pEGFP-N1 or pSARS-CoV-PLpro plus pEGFP-N1 were selected by a 2-week incubation with G418. The HSV-tag fusion protein was detected using immunofluorescence staining of anti-HSV tag antibody and rhodamineconjugated antimouse IgG antibody (A). Lysates from cells transfected with pcDNA3.1 plus pEGFP-N1 (lane 1) or pSARS-CoV-PLpro plus pEGFP-N1 (lane 2) were analyzed by 10% SDS-PAGE prior to blotting (B). The blot's upper half of was probed with anti-HSV antibody, the lower with anti-β actin antibody as internal control. Trans-cleavage activity of SARS-CoV PLpro in transfected cell lysates was further analyzed (C). Following incubation of lysates from 10^6 PLpro-expressing cells and control vector cells with substrate HRP, residual HRP activity was measured as a mean of 3 independent experiments; error bars show standard error of the mean

Fig. 2. Effect of PLpro on ISRE mediated gene expression in response to IFNα. (A) Vector control cells and PLro-expressing cells were transiently co-transfected with reporter plasmid containing firefly luciferase under control of the ISRE and an internal control reporter pRluc-C1 that constitutively expressed *Renilla* luciferase. After 4-hour IFNαtreatment, firefly luciferase and renilla luciferase were measured and firefly luciferase activity normalized to *Renilla* luciferase activity, as reported. Each bar is the mean of 3 independent experiments; error bar is standard error of the mean. The mRNA expressions of ISRE-driven gene PKR (B) and 2'-5'-OAS (C) in vector control cells and SARS PLpro-expressing cells

untreated or treated was measured by quantitative real time PCR. Relative fold levels of PKR or 2'-5'-OAS mRNA level appear as ratio of PKR or 2'-5'-OAS mRNA/GAPDH mRNA. Each bar graph is the mean of 3 independent experiments; error bars represent standard error of the mean.

Fig. 3. Effect of PLpro on AP-1 mediated gene expression in response to IFNα. (A) Vector control and PLpro-expressing cells were transiently co-transfected with reporter plasmid containing AP-1-driven firefly luciferase and an internal control reporter pRluc-C1 that constitutively expressed renilla luciferase. After 4-hour treatment with IFNα, AP-1-driven firefly luciferase and renilla luciferase were measured and firefly luciferase activity normalized to renilla luciferase activity is reported. Each bar is the mean of 3 independent experiments; error bar is standard error of the mean. In addition, the mRNA expressions of AP-1-driven genes IL-6 (B) and IL-8 (C) in vector control cells and SARS PLpro-expressing cells untreated or treated was measured by quantitative real time PCR. Relative fold levels of IL-6 or IL-8 mRNA level are presented as the ratio of IL-6 or IL-8 mRNA/GAPDH mRNA. Each bar on the graph is the mean of 3 independent experiments; error bars represent standard error of the mean.

Fig. 4. Effect of SARS-CoV PLpro on protein profiles of vector control cells and PLpro-expressing cells in response to IFNα. 100 μg of total protein from control vector cells in the absence or presence of IFNα or PLpro-expressing cells in the absence or presence of IFNα was resolved by 2-dimensional electrophoresis. (A) Enlarged images of two-dimensional gel electrophoresis of protein expression in PLpro-expressing cells and vector control cells in response to IFNα treatment. (B)

Nanoelectrospray mass spectrum of triply charged ion m/z 1514.77 for ERK1 is shown; ITVEEALAHPYLEQYYDPTDEPVAEEPFTFAM$_{ox}$ELDDLPK amino acid sequence was determined from mass differences in y- and b-fragment ions series and matched residues 319-357 of ERK1 (mitogen-activated protein kinase 3). (C) Nanoelectrospray mass spectrum of the doubly charged ion m/z 725.41 for UBC E2-25k is shown. Amino acid sequence VDLVDENFTELR was determined from mass differences in y- and b-fragment ions series and matched residues 29-40 of ubiquitin-conjugating enzyme E2-25k. *Only y- and b-fragment ions are labeled in the spectrum.

Fig. 5. Analysis of mRNA levels of ERK1 and UBC E2-25K in vector control cells and PLpro-expressing cells. Total RNA was extracted from vector control cells and PLpro-expressing cells treated with or without IFNα (3000U/ml) for 4 hrs and relative mRNA levels of ERK1 (A) and UBC E2-25K (B) were measured by quantitative real time PCR. The relative fold levels of ERK1 and UBC E2-25K mRNA were presented as the ratio of indicated mRNA/GAPDH mRNA. Each bar on the graph is the mean of 3 independent experiments and the error bars represent the standard error of the mean.

Fig. 6. Protein amount and ubiquitination level of ERK1 in vector control cells and PLpro-expressing cells. (A) Vector control cells and PLpro-expressing cells were treated with IFNα (3000U/ml) for 30 or 60 minutes. Cell lysates were Western blotted and probed with anti-ERK1/2 or anti-β-actin antibody as an internal control. (B) Vector control cells and PLpro-expressing cells were treated with or without IFNα (3000U/ml) for 60 minutes. Cell lysates were also

immunoprecipitated with anti-ERK1 mAb, followed by Western blotting probed with either anti-ubiquitin or anti-ERK1 antibody. (C) Vector control cells and PLpro-expressing cells were treated with IFNα and the proteosome inhibitor MG132 (20μM) for 10, 30, or 60 minutes. Cell lysates were Western blotted and probed with anti-ERK1/2 or anti-β-actin antibody as an internal control.

Fig. 7. Effect of proteasome inhibitor MG132 on IFNα-induced phosphorylation of ERK1, STAT1 and c-Jun in vector control cells and PLpro-expressing cells. Vector control cells and PLpro-expressing cells were treated with IFNα (3000U/ml) (A), or IFNα and proteasome inhibitor MG132 (20μM) (B) for 10, 30 or 60 minutes. Cell lysates were subjected to Western blotting probed with anti-phospho-ERK1/2, anti-ERK1/2 anti-phospho-STAT1 (Tyr701), anti-phospho-STAT1 (Ser727), anti-STAT1, anti-phospho-c-Jun or anti-c-Jun antibodies. Relevant protein of the blot was probed with anti-β actin antibodies as an internal control.

Fig. 8. Effect of PD098059 treatment on IFNα-induced phosphorylation of ERK1 and STAT1 in vector control cells and PLpro-expressing cells. Vector control cells and PLpro-expressing cells were treated with IFNα (A), or IFNα and PD098059 (B) for 10, 30 or 60 minutes. Cell lysates were subjected to Western blotting probed with anti-phospho-ERK1/2, anti-ERK1/2, anti-phospho-STAT1 (Tyr701), anti-phospho-STAT1 (Ser727) or anti-STAT1 antibodies. Relevant protein of the blot was probed with anti-β actin antibodies as an internal control.

Fig 1A

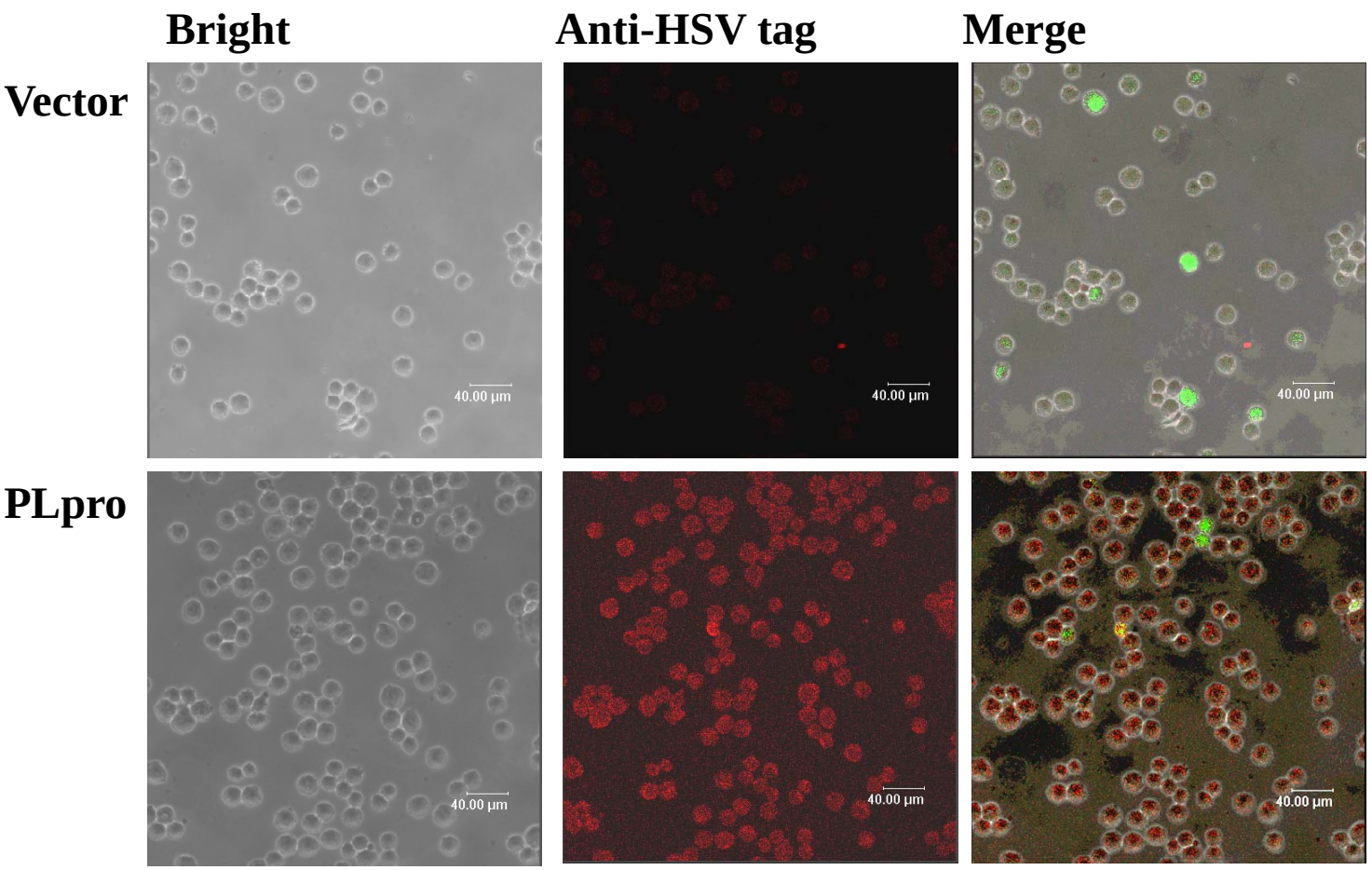

Fig. 1B

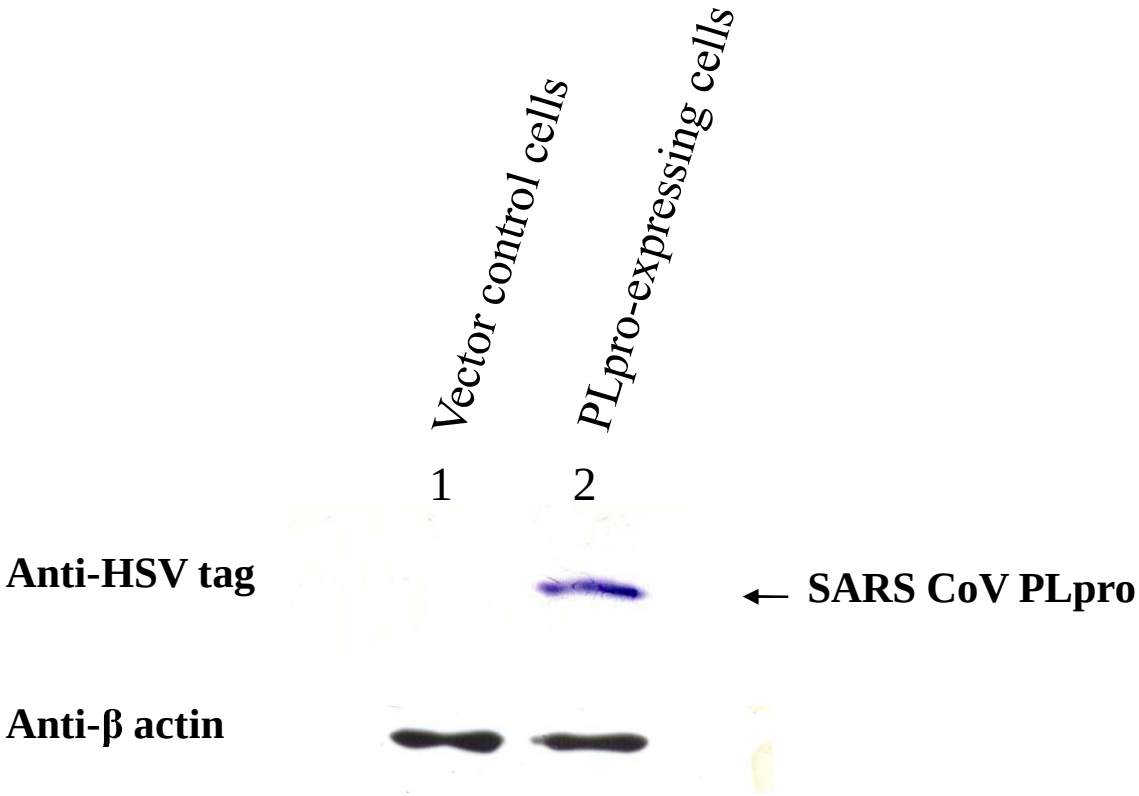
Vector control cells
PLpro-expressing cells
1
2
Anti-HSV tag
SARS CoV PLpro
Anti-β actin

Fig. 1C

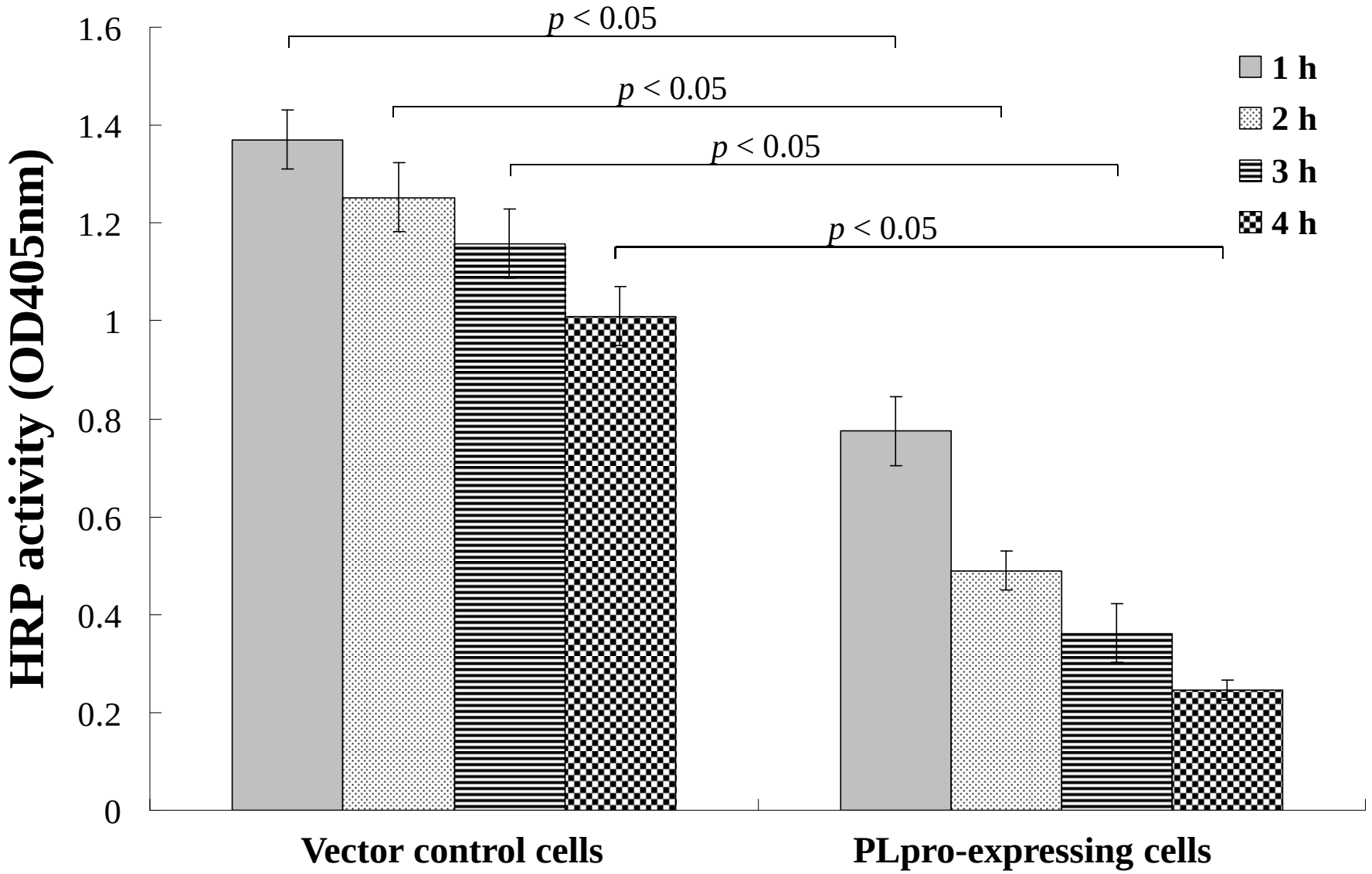
p < 0.05
p < 0.05
p < 0.05
p < 0.05
1 h
2 h
3 h
4 h
HRP activity (OD405nm)
1.6
1.4
1.2
1
0.8
0.6
0.4
0.2
0
Vector control cells
PLpro-expressing cells

Fig. 2A

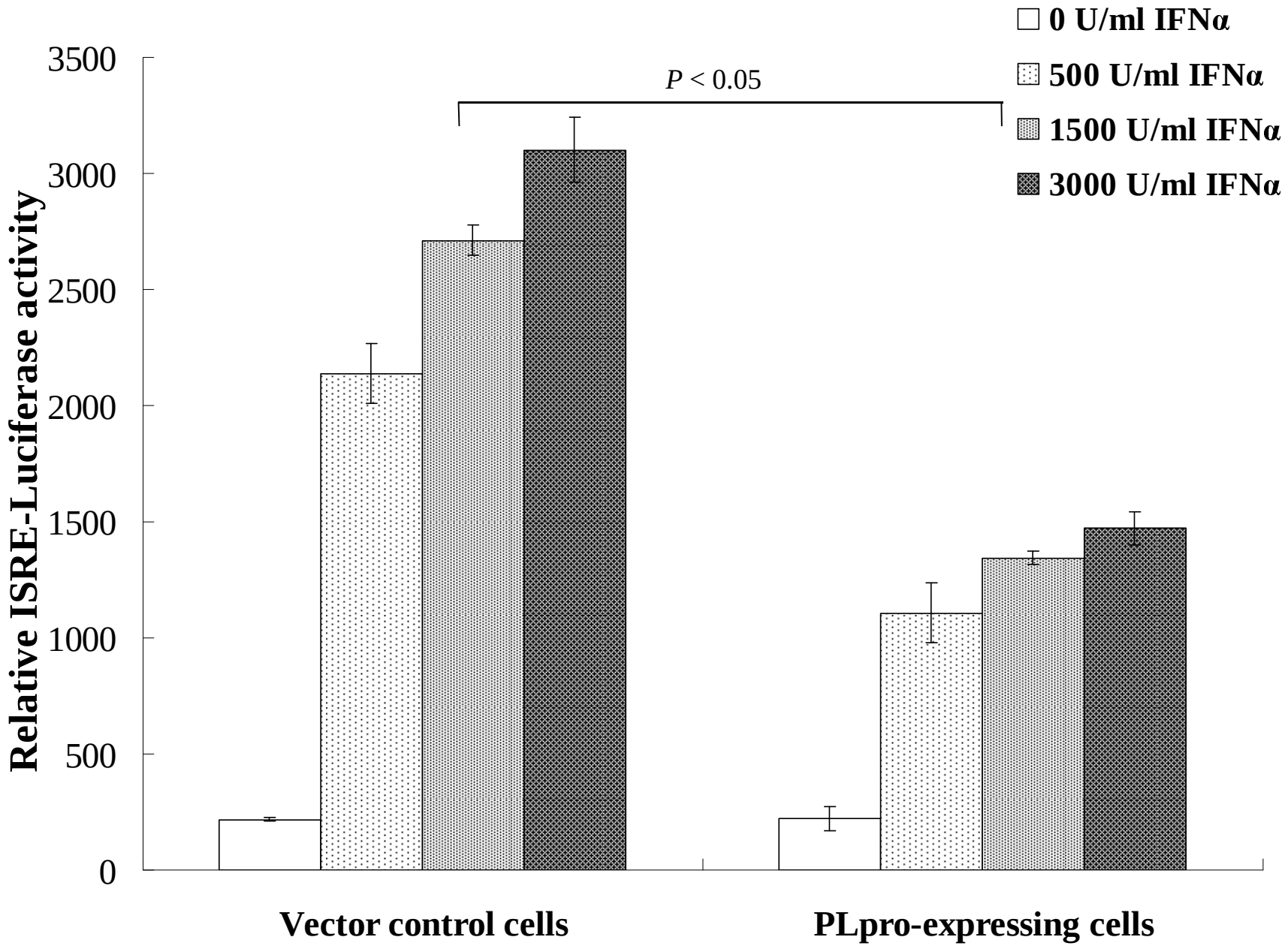
0 U/ml IFNα
500 U/ml IFNα
1500 U/ml IFNα
3000 U/ml IFNα
P < 0.05
Relative ISRE-Luciferase activity
3500
3000
2500
2000
1500
1000
500
0
Vector control cells
PLpro-expressing cells

Fig. 2B

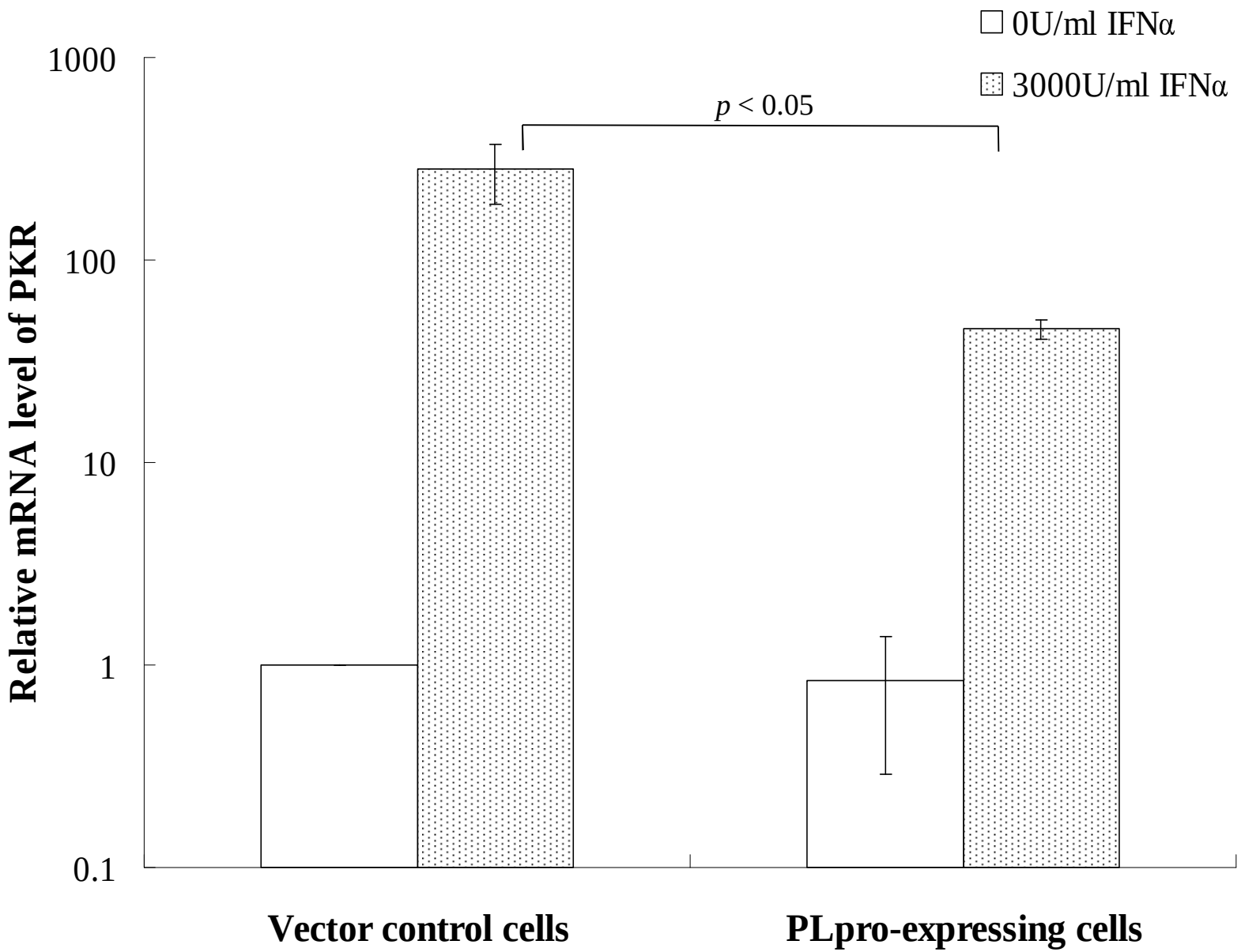
0U/ml IFNα
3000U/ml IFNα
p < 0.05
1000
100
10
1
0.1
Relative mRNA level of PKR
Vector control cells
PLpro-expressing cells

Fig. 2C

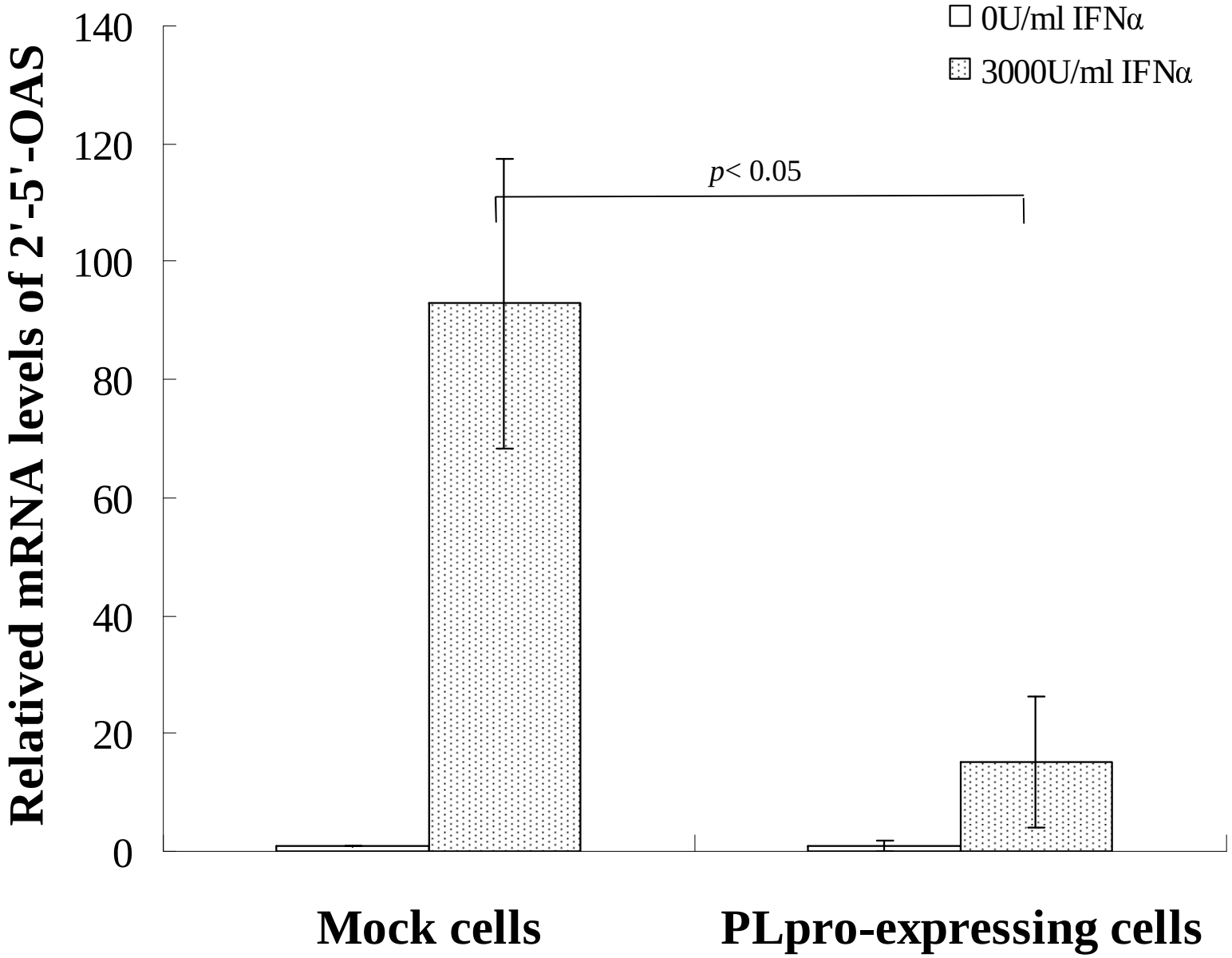
0U/ml IFNα
3000U/ml IFNα
Relatived mRNA levels of 2'-5'-OAS
140
120
100
80
60
40
20
0
p< 0.05
Mock cells
PLpro-expressing cells

Fig. 3A

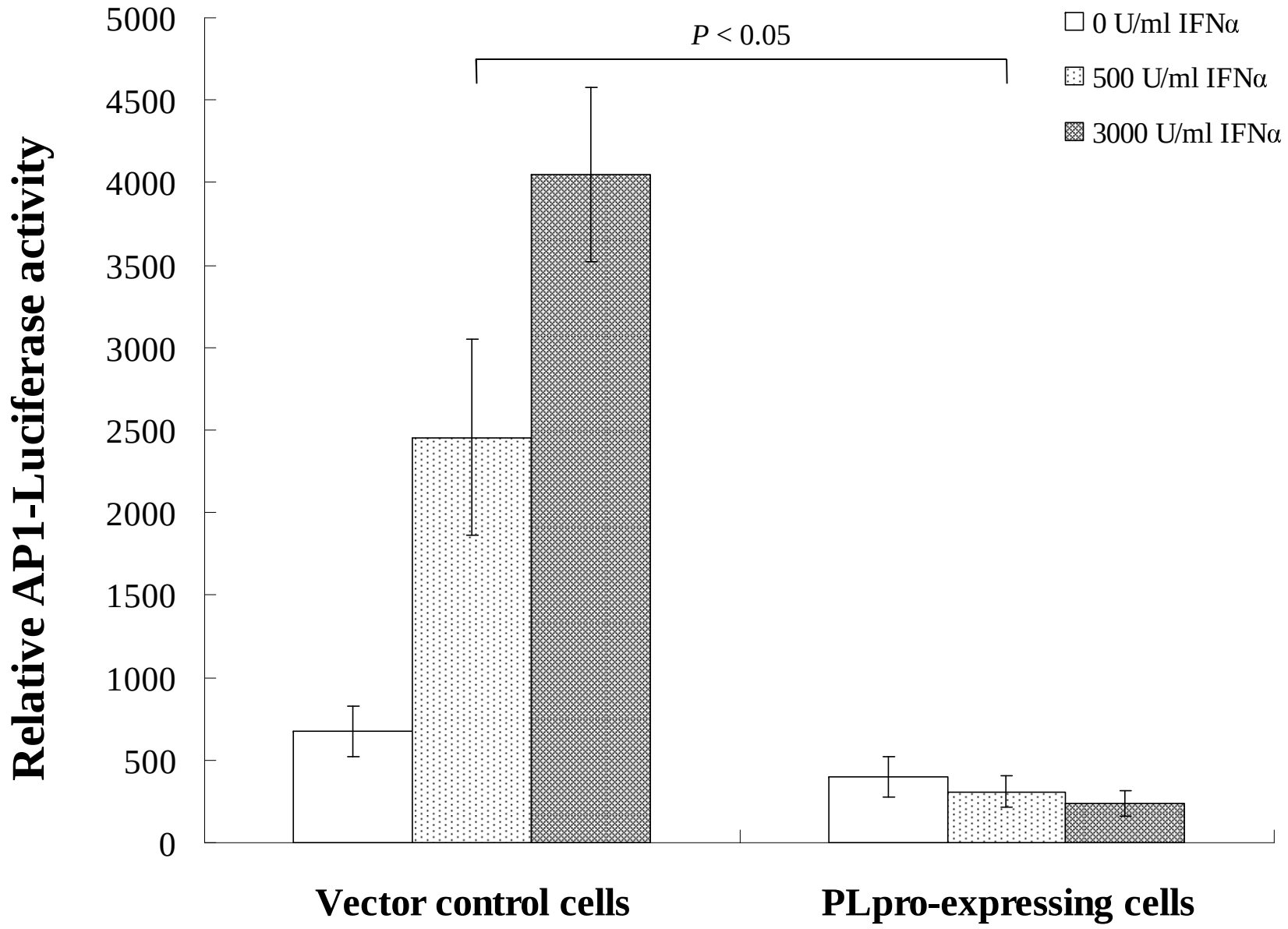
Relative AP1-Luciferase activity
5000
4500
4000
3500
3000
2500
2000
1500
1000
500
0
P < 0.05
0 U/ml IFNα
500 U/ml IFNα
3000 U/ml IFNα
Vector control cells
PLpro-expressing cells

Fig. 3B

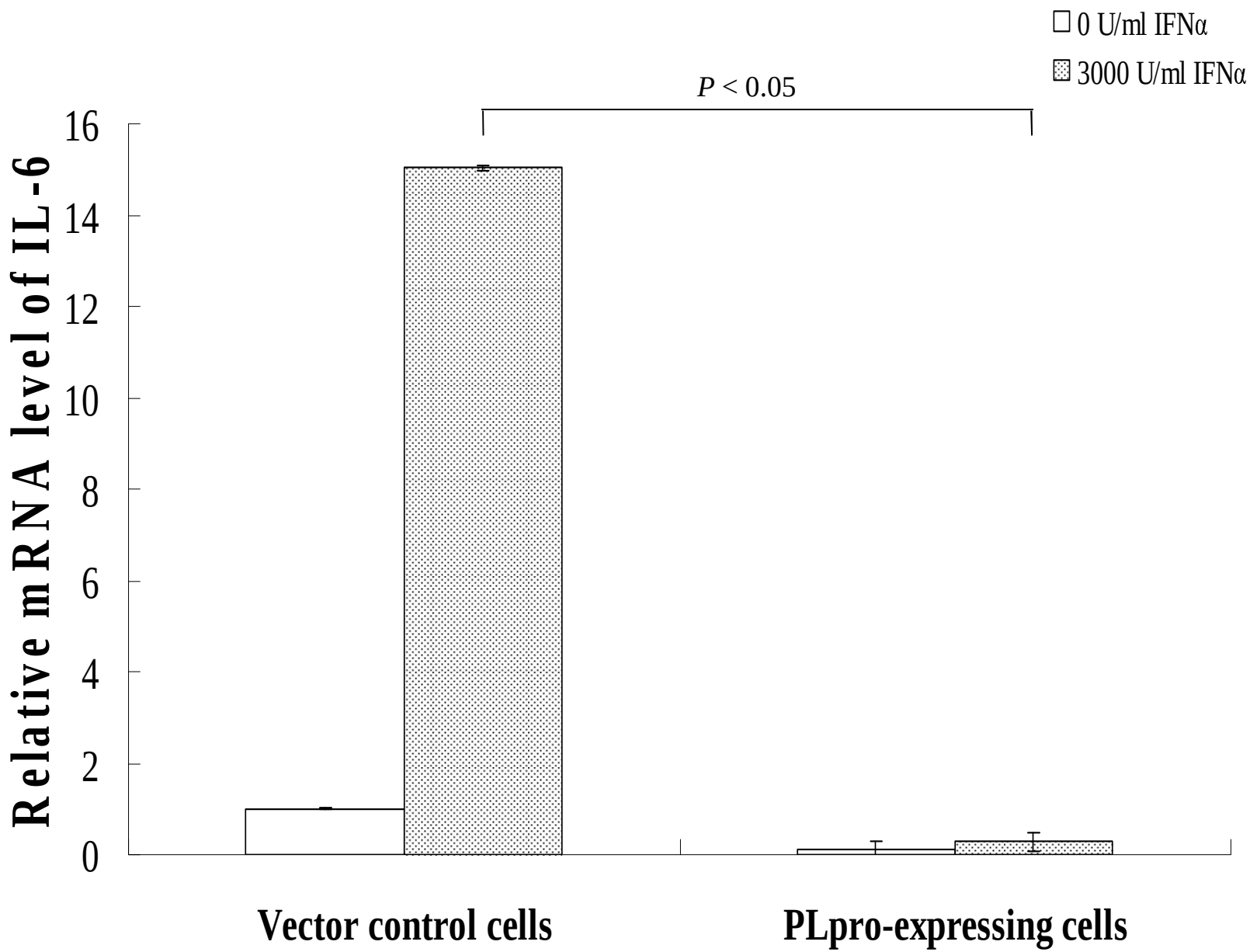
0 U/ml IFNα
3000 U/ml IFNα
P < 0.05
Relative mRNA level of IL-6
16
14
12
10
8
6
4
2
0
Vector control cells
PLpro-expressing cells

Fig. 3C

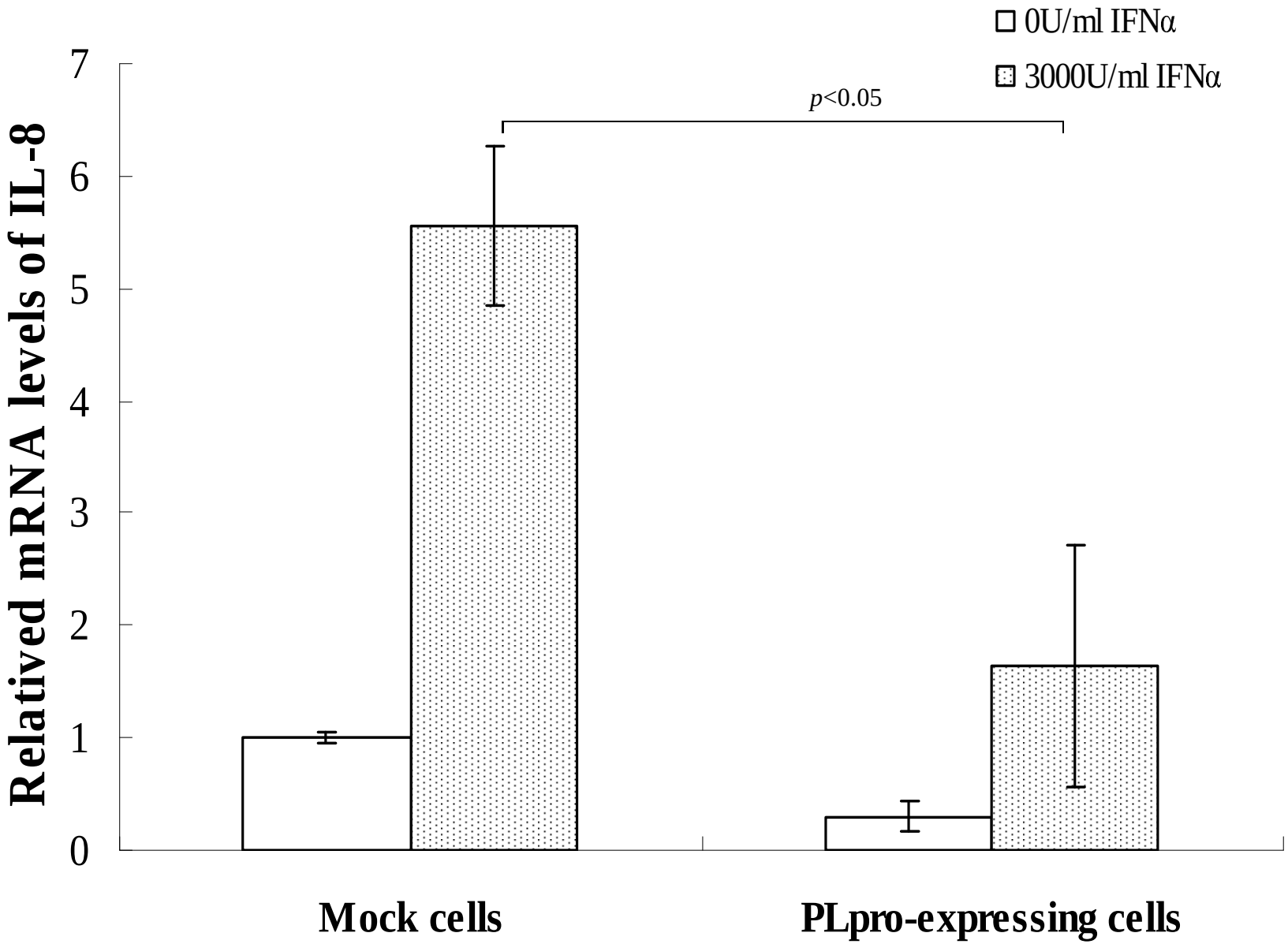
0U/ml IFNα
3000U/ml IFNα
p<0.05
Relatived mRNA levels of IL-8
0
1
2
3
4
5
6
7
Mock cells
PLpro-expressing cells

Fig. 4A

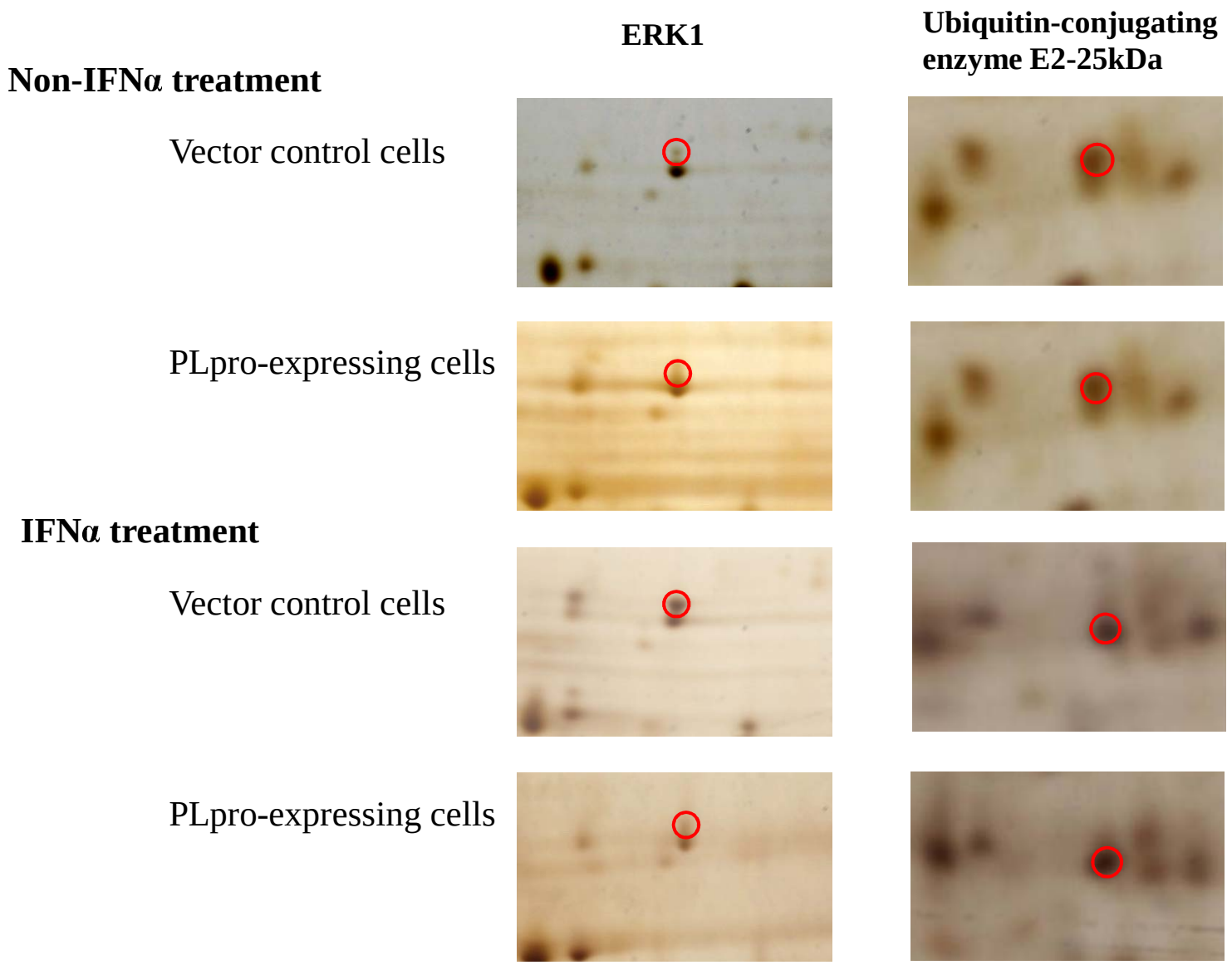
ERK1
Ubiquitin-conjugating enzyme E2-25kDa
Non-IFNα treatment
Vector control cells
PLpro-expressing cells
IFNα treatment
Vector control cells
PLpro-expressing cells

Fig. 4B

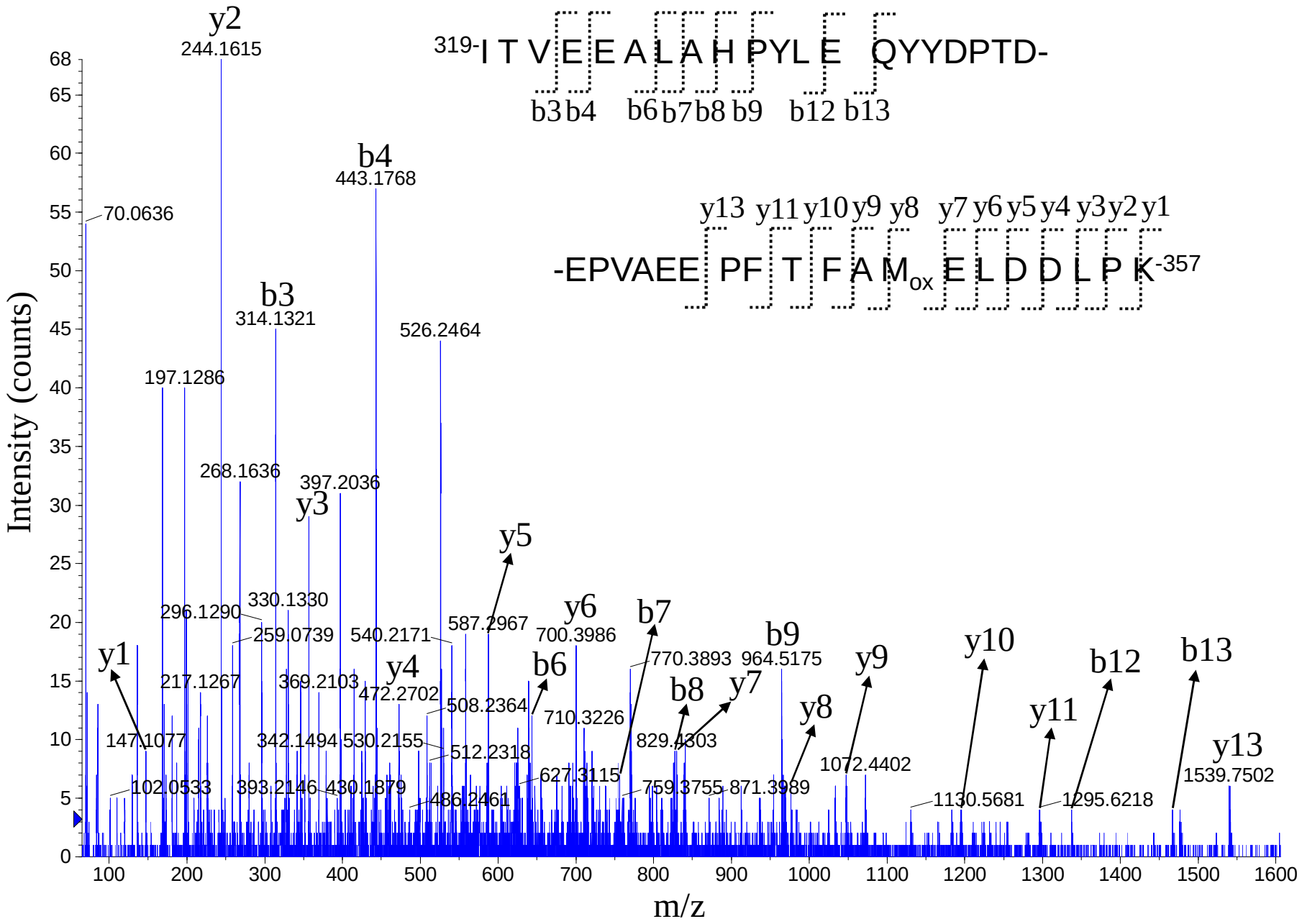
319-I T V E E A L A H P Y L E Q Y Y D P T D-
b3 b4 b6 b7 b8 b9 b12 b13
y13 y11 y10 y9 y8 y7 y6 y5 y4 y3 y2 y1
-E P V A E E P F T F A M ox E L D D L P K-357
Intensity (counts)
m/z
y2
244.1615
b4
443.1768
70.0636
b3
314.1321
526.2464
197.1286
268.1636
397.2036
y3
y5
330.1330
296.1290
259.0739
540.2171
587.2967
y6
700.3986
b7
770.3893
b9
964.5175
y9
y10
b12
b13
y1
y4
b6
b8
y7
y8
y11
y13
217.1267
369.2103
472.2702
508.2364
710.3226
829.4303
1072.4402
1539.7502
147.1077
342.1494
530.2155
512.2318
627.3115
759.3755
871.3989
1130.5681
1295.6218
102.0533
393.2146
430.1879
486.2461

Fig. 4C

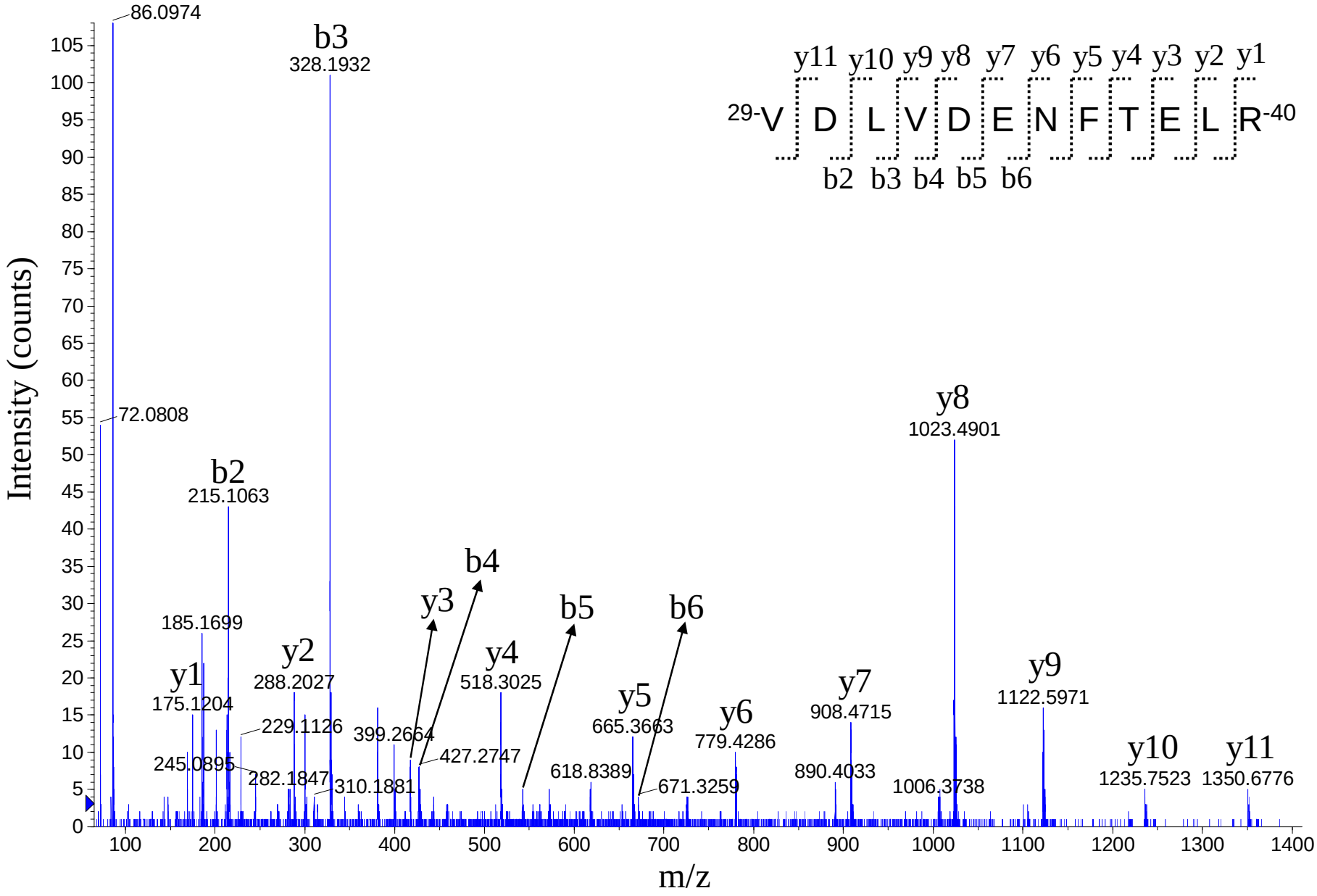
y11 y10 y9 y8 y7 y6 y5 y4 y3 y2 y1
29-V D L V D E N F T E L R-40
b2 b3 b4 b5 b6
Intensity (counts)
m/z
86.0974
b3
328.1932
72.0808
b2
215.1063
y8
1023.4901
b4
y3
b5
b6
185.1699
y2
288.2027
y4
518.3025
y1
175.1204
y5
665.3663
y6
779.4286
y7
908.4715
y9
1122.5971
229.1126
399.2664
427.2747
245.0895
282.1847
310.1881
618.8389
671.3259
890.4033
1006.3738
y10
1235.7523
y11
1350.6776

Fig. 5A

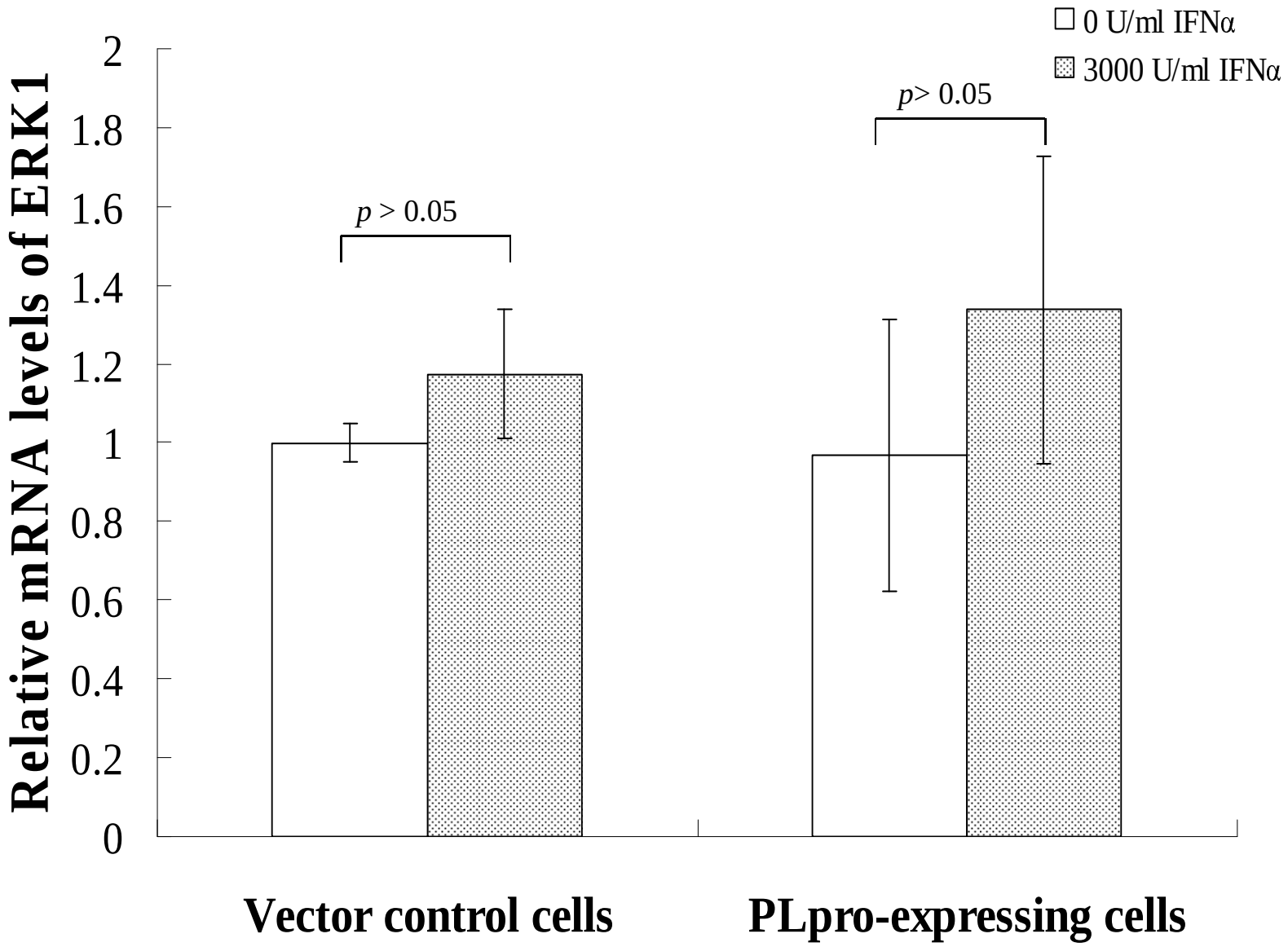
0 U/ml IFNα
3000 U/ml IFNα
p> 0.05
p > 0.05
Relative mRNA levels of ERK1
2
1.8
1.6
1.4
1.2
1
0.8
0.6
0.4
0.2
0
Vector control cells
PLpro-expressing cells

Fig. 5B

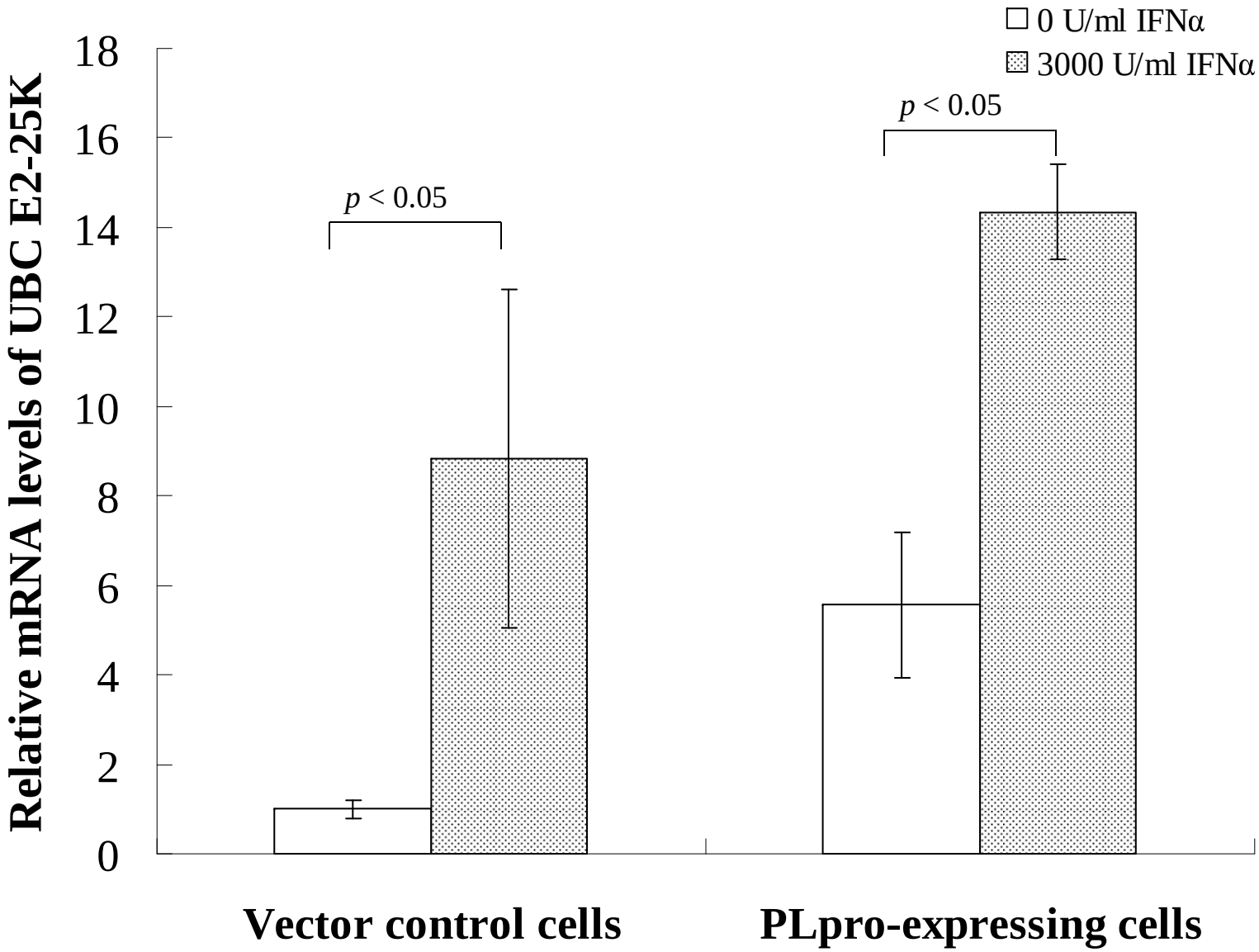
0 U/ml IFNα
3000 U/ml IFNα
p < 0.05
p < 0.05
Relative mRNA levels of UBC E2-25K
18
16
14
12
10
8
6
4
2
0
Vector control cells
PLpro-expressing cells

Fig. 6A

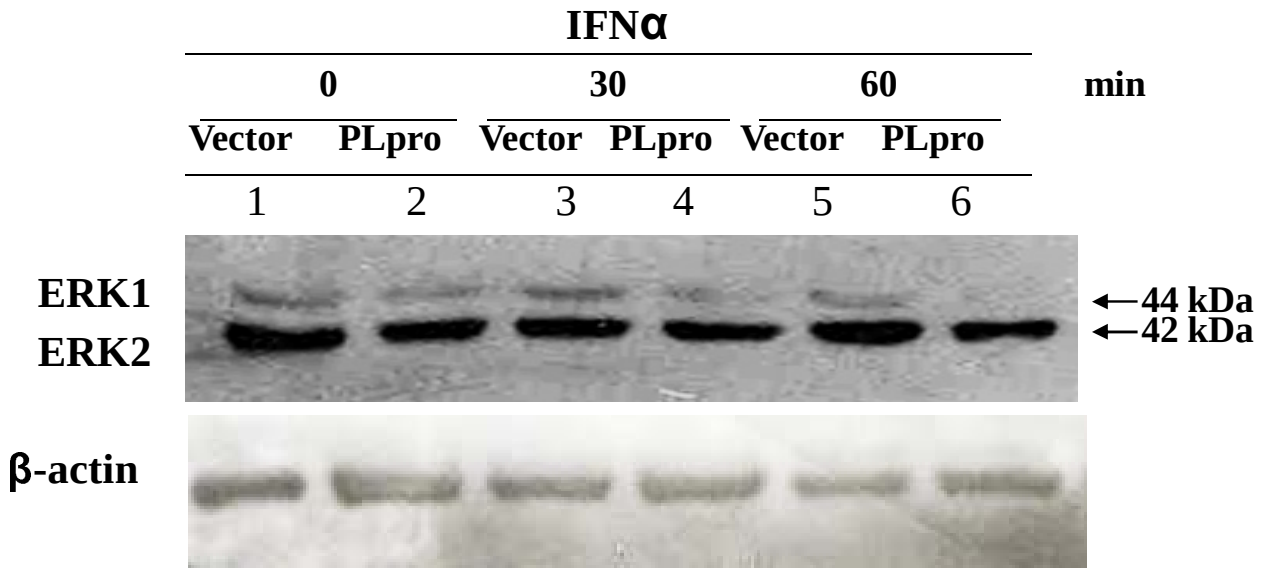
IFNα
0
30
60
min
Vector
PLpro
Vector
PLpro
Vector
PLpro
1
2
3
4
5
6
ERK1
ERK2
β-actin
44 kDa
42 kDa

Fig. 6B

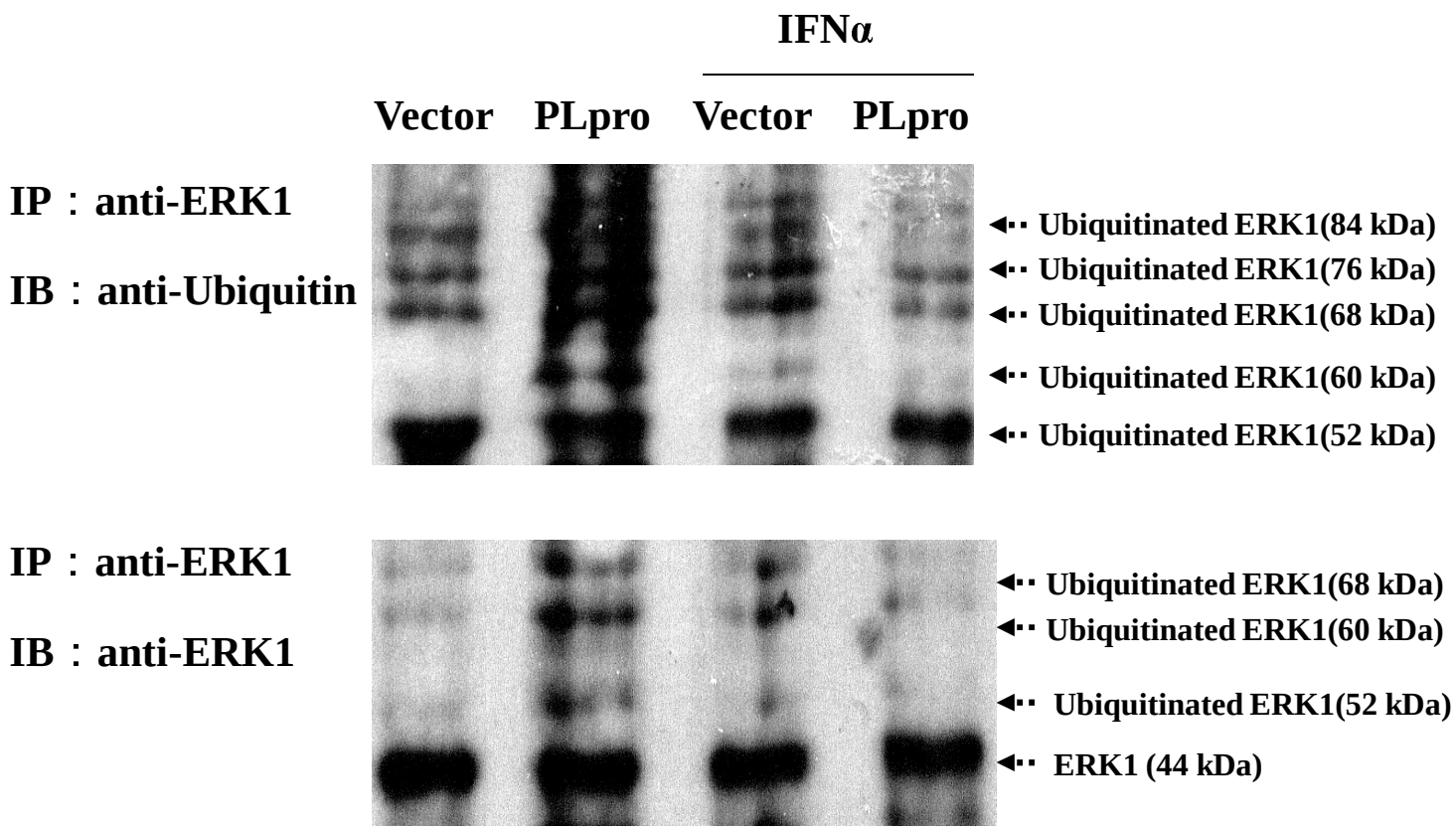
IFNα
Vector
PLpro
Vector
PLpro
IP：anti-ERK1
IB：anti-Ubiquitin
Ubiquitinated ERK1(84 kDa)
Ubiquitinated ERK1(76 kDa)
Ubiquitinated ERK1(68 kDa)
Ubiquitinated ERK1(60 kDa)
Ubiquitinated ERK1(52 kDa)
IP：anti-ERK1
IB：anti-ERK1
Ubiquitinated ERK1(68 kDa)
Ubiquitinated ERK1(60 kDa)
Ubiquitinated ERK1(52 kDa)
ERK1 (44 kDa)

Fig 6C

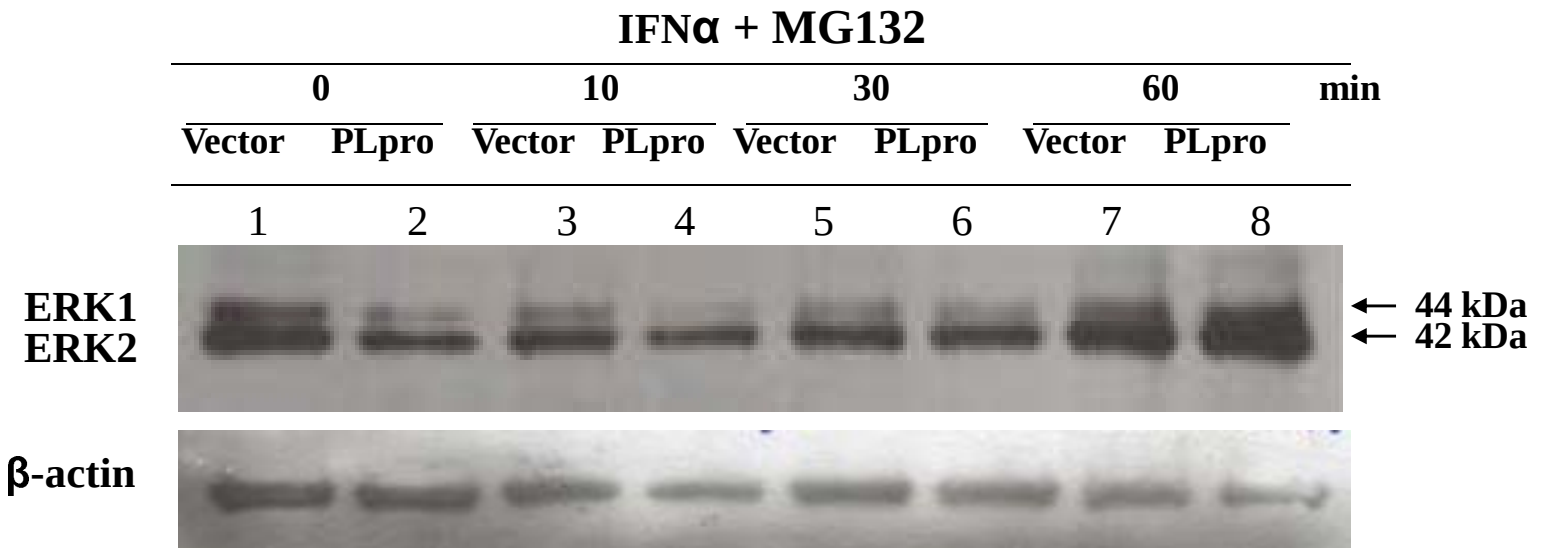
IFNα + MG132
0
10
30
60
min
Vector
PLpro
Vector
PLpro
Vector
PLpro
Vector
PLpro
1
2
3
4
5
6
7
8
ERK1
ERK2
β-actin
44 kDa
42 kDa

Fig. 7A

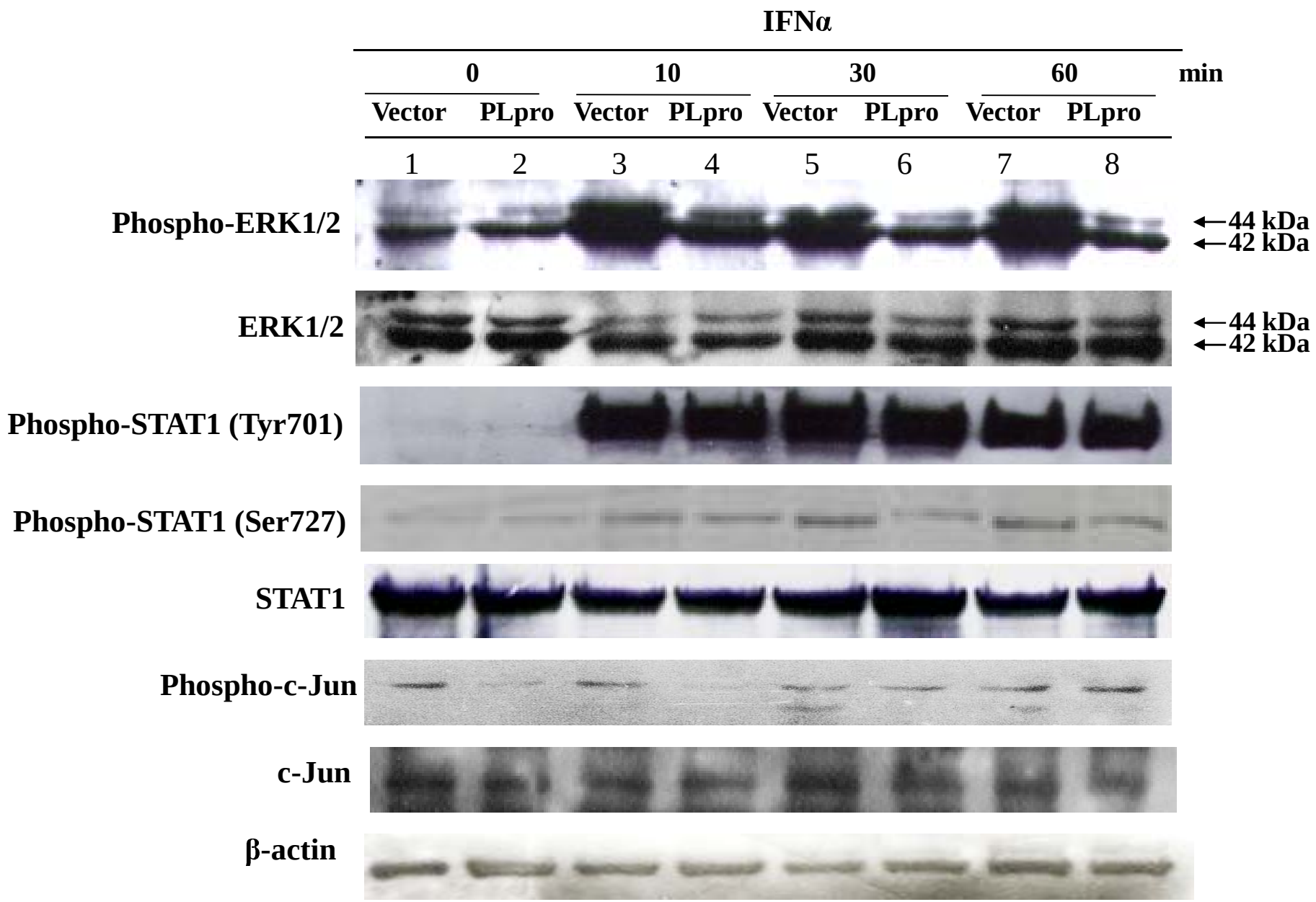
IFNα
0
10
30
60
min
Vector
PLpro
Vector
PLpro
Vector
PLpro
Vector
PLpro
1
2
3
4
5
6
7
8
Phospho-ERK1/2
←44 kDa
←42 kDa
ERK1/2
←44 kDa
←42 kDa
Phospho-STAT1 (Tyr701)
Phospho-STAT1 (Ser727)
STAT1
Phospho-c-Jun
c-Jun
β-actin

Fig 7B

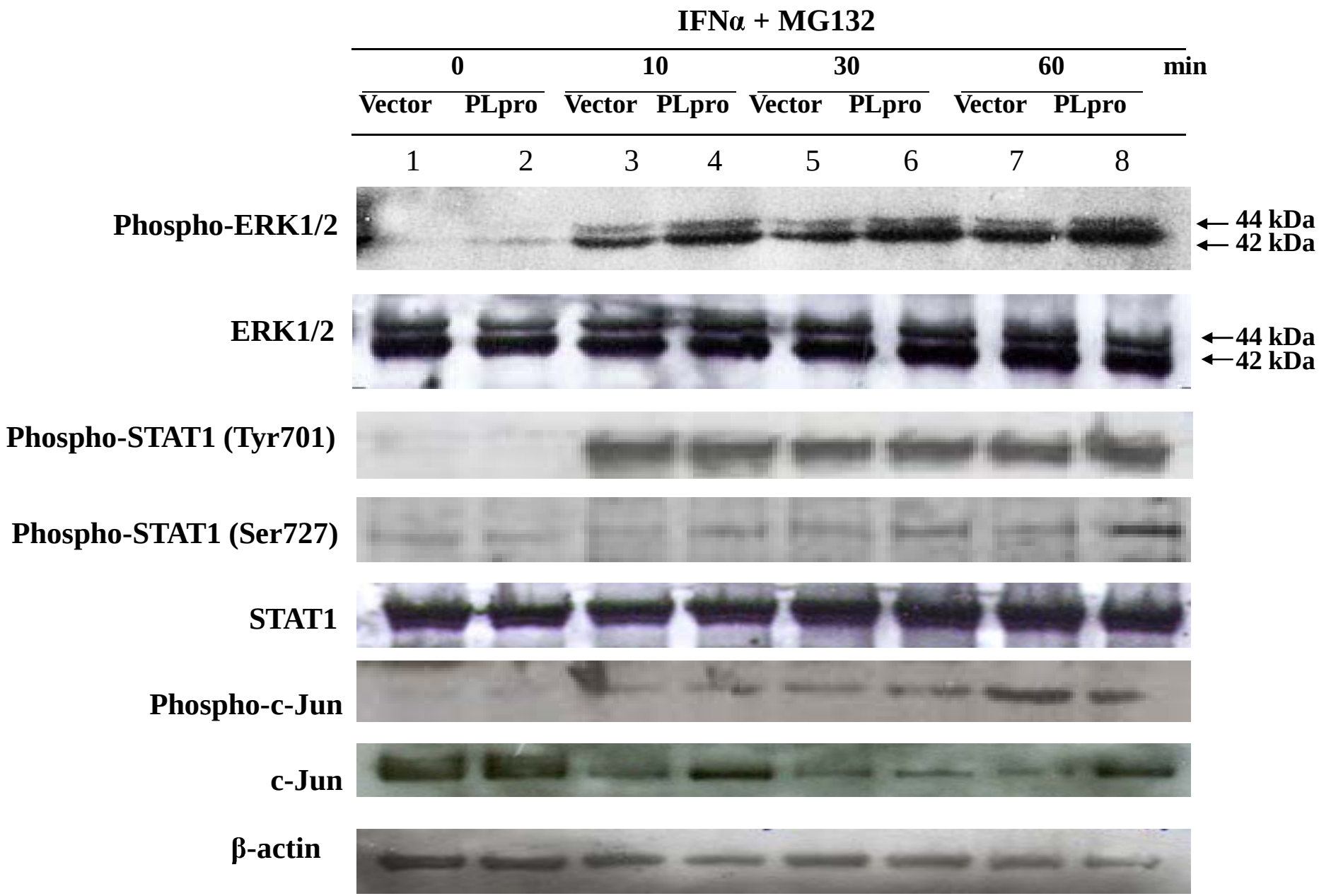
IFNα + MG132
0
10
30
60
min
Vector
PLpro
Vector
PLpro
Vector
PLpro
Vector
PLpro
1
2
3
4
5
6
7
8
Phospho-ERK1/2
44 kDa
42 kDa
ERK1/2
44 kDa
42 kDa
Phospho-STAT1 (Tyr701)
Phospho-STAT1 (Ser727)
STAT1
Phospho-c-Jun
c-Jun
β-actin

Fig 8A

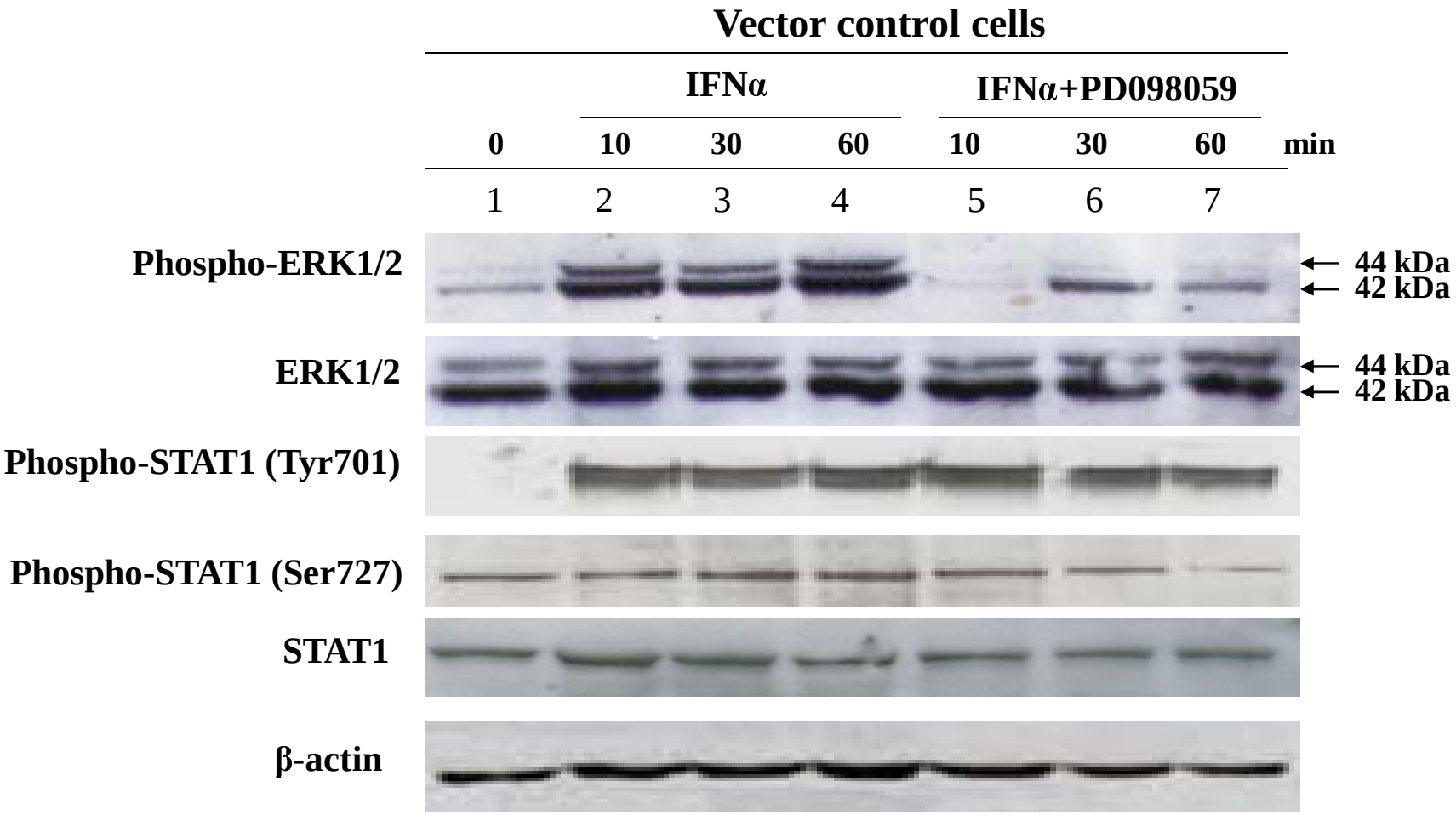
Vector control cells
IFNα
IFNα+PD098059
0
10
30
60
10
30
60
min
1
2
3
4
5
6
7
Phospho-ERK1/2
44 kDa
42 kDa
ERK1/2
44 kDa
42 kDa
Phospho-STAT1 (Tyr701)
Phospho-STAT1 (Ser727)
STAT1
β-actin

Fig 8B

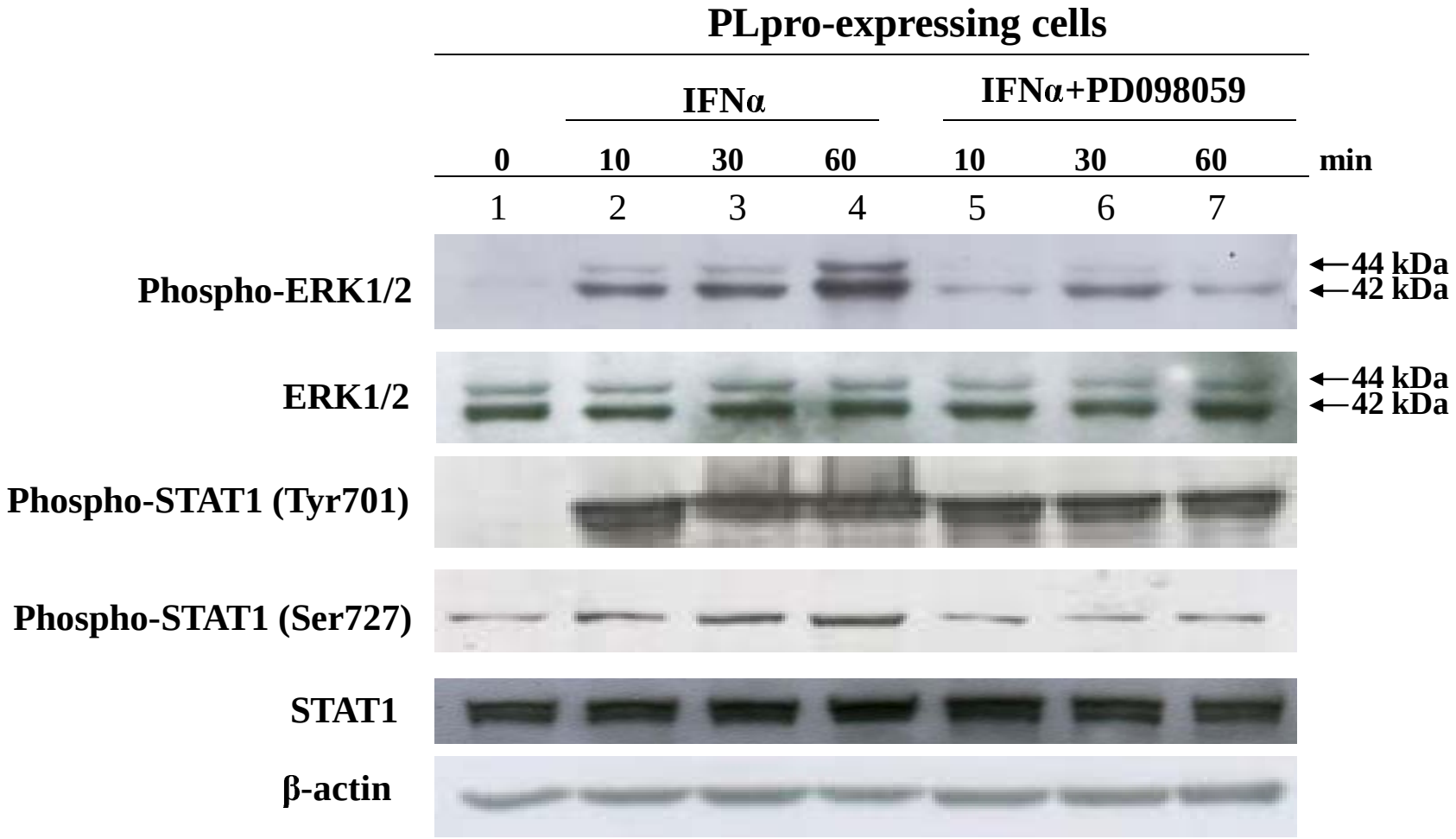
PLpro-expressing cells
IFNα
IFNα+PD098059
0
10
30
60
10
30
60
min
1
2
3
4
5
6
7
Phospho-ERK1/2
ERK1/2
Phospho-STAT1 (Tyr701)
Phospho-STAT1 (Ser727)
STAT1
β-actin
←44 kDa
←42 kDa
←44 kDa
←42 kDa